Космични изследвания в България

Том 6 . София . 1990

Българска академия на науките

Address

Space Research in Bulgaria
Space Research Institute
Bulgaria, 1000 Sofia, 1 Rouski Bld.

Адрес

Космични изследвания в България
Институт за космически изследвания
1000 София, бул. „Руски“ № 1

Издателство на Българската академия на науките

Редактор *Лидия Шведова* Технически редактор *Зара Зидрова* Коректор *Людмила Събева*
Изд. индекс 11202 Дадена за набор на 30. VIII. 1989 Подписана за печат на 30. III. 1990 г.
Излязла от печат на 16. IV. 1990 г. Формат 70×100/16 Тираж 540 Печатни коли 4,88
Издателски коли 6,32 УИК 7,08 Цена 1,20 лв. Поръчка № 28

Код 28 $\frac{9532422211}{2332\text{-}3\text{-}90}$

Печатница на Издателството на БАН — 1113 София, ул. „Акад. Г. Бончев“, бл. 6

ISSN 0204-9104

Space Research in Bulgaria

Volume 6. Sofia. 1990

Bulgarian Academy of Sciences

Contents

G. G. Shepherd, I. S. Kutiev — Optical emissions in the nighttime subauroral region during the March 1-4, 1982 magnetic storm 3
K. B. Serafimov, M. K. Serafimova — Effects of the topside ionosphere on radiowaves propagation from space objects 12
L. G. Filipov — On self-similar solutions in disk accretion problems 21
A. Z. Bochev, S. T. Hadjistoyanov, N. B. Istatkov, H. M. Georgiev. A computing programme for coordinate transformation of vector magnetometer data 29
V. S. Petrova — A complex satellite experiment of investigating aerosolic optical properties in the atmosphere 34
D. N. Mishev, A. M. Angelov, G. H. Mardirosyan, B. H. Tsenov, M. F. Fratev, A. K. Madjirov — Data acquisition system for complex and synchronous geonomic and space investigations . 40
N. P. Petkov — Interference light filter shifting device for the EMO-5 satellite photometric system 45
P. T. Baynov, Y. V. Semkova — Systems for laboratory testing of two-dimensional coordinate-sensitive detectors for charged particles 50
M. N. Gousheva — Device for measurement of current and voltage differences 55
Y. B. Dimitriev, J. M. Simeonova — On some specifics in the selection of glass material for microchannel plates in space applications . . . 59
N. B. Tabov, I. A. Kurtev — Functional generator capacity increase via new building elements 62
A. G. Gentchev — Increase of the efficiency of self-oscillating push-pull power converter 67
S. I. Sargoichev — A controllable device for the two-dimensional scanner in the three-channel spectrometer for the VEGA mission 73

Содержание

Г. Г. Шепард, И. С. Кутиев — Оптические эмиссии в ночной субавроральной области во время мартовской бури 1—4 марта 1982 г. 11
К. Б. Серафимов, М. К. Серафимова — Воздействия внешней ионосферы на распространение радиоволн из космических объектов . . . 20

Л. Г. Филипов — Об автомодельных решениях задачи дисковой акреции . 28
А. З. Бочев, С. Ц. Хаджистоянов, Н. Б. Истатков, Х. М. Георгиев — Программа ЭВМ о координатных трансформациях при замерах вектора магнитного поля 33
В. Д. Петрова — Комплексный спутниковый эксперимент по исследованию оптических свойств аэрозоля в атмосфере 39
Д. Н. Мишев, А. М. Ангелов, Г. Х. Мардиросян, Б. Х. Ценов, М. Ф. Фратев, А. К. Маджиров — Система сбора данных в комплексных и синхронных геономических исследованиях . . 44
Н. П. Петков — Устройство для перемещения интерференционных светофильтров в спутниковой фотометрической системе ЭМО—5 49
П. Т. Байнов, Й. В. Семкова — Система лабораторных испытаний двухмерных координатно-чувствительных детекторов заряженных частиц . 54
М. Н. Гушева — Устройство для измерения разности тока и напряжения . 58
Я. Б. Димитриев, Ю. М. Симеонова — О некоторых особенностях при выборе стекла для микроканальных пластин, работающих в космосе 61
Н. Б. Табов, И. Ал. Куртев — Расширение возможностей функциональных генераторов при использовании новых градивных элементов . 66
А. Г. Генчев — Повышение коэффициента полезного действия самоосциллирующего двухтактного преобразователя мощности 72
С. И. Саргойчев — Управляющее устройство двухмерного сканера в аппаратуре „Триканальный спектрометр“ на станциях „Вега“ 78

The present issue No 6 of the *Space Research* series was delayed owing to circumstances beyond the control of the Editorial Board of the series.

BAS Publishing House

Bulgarian Academy of Sciences

Space Research in Bulgaria, 6

Sofia . 1990

Optical emissions in the nighttime subauroral region during the March 1-4, 1982 magnetic storm

*Cordon G. Shepherd, Ivan S. Kutiev**

York University, 4700 Keele St., North York, Ontario, Canada M3J 1p3
**Geophysical Institute, Bulgarian Academy of Sciences*

Introduction

Cole suggested in 1965 that stable auroral red (SAR) arc was a sink for ring current energy [1], but progress has been slow in identifying the mechanism for getting the ring current energy into the ionosphere. A major advance was made recently [4] in directly observing from the DYNAMICS EXPLORER-2 satellite at 850 km the heated electron population responsible for the 6300 Å emission. It was characterized as having a temperature of 9900° K, and a bulk velocity of 275 km/s. Authors of [5] confirmed that this population could excite the SAR arc observed from the ground at the same time. In [4] was also found that the heated population was not recorded by the DE-1 satellite, at 6000 km altitude on the same field line, which suggests that the heating is more local than expected for a ring current source. Finally, it was noted that photoelectrons produced in the sunlit conjugate hemisphere were blocked from reaching the dark hemisphere in the region of the SAR arc. This suggests that the two hemispheres were electrically disconnected in the SAR arc.

The present study is aimed at extending the ideas developed in previous papers. The INTERCOSMOS-BULGARIA-1300 satellite provides detailed measurements of the atomic oxygen emissions at 5577 Å and 6300 Å, as well as the N_2^+ 4278 Å emission and the hydrogen Balmer beta 4861 Å emission. Both electrons and photons are observed, down to energies of 200 eV; this does not permit observation of the suprathermal population but serves well to define the auroral oval boundaries. Closely coincident DE-2 passes are used to relate the suprathermal electron population to the BULGARIA-1300 data. The soft precipitation region equatorward of the oval can overlap into the SAR arc region, thus making it difficult to distinguish between the auroral (factually subauroral) energy source and the ring current source. This is considered in detail using a number of examples.

Attention is given to plasma drifts in the region of the SAR arc, and the SAR arc phenomenon is compared with conditions during penetration of the convection electric field into the subauroral region, as discussed in [6]. The author has established, for example, a close correlation between increasing drift velocity and increasing temperature, which also occurs in association with a trough in the ion density and the presence of suprathermal electrons. This phenomenon occurs just beyond the equatorward boundary of the oval. However, as it was already noted, these regions can overlap, which could make them indistinguishable. An important consequence is that the suprathermal electrons observed during electric field penetration can occur in the absence of a ring current. The problem is whether there can be two different mechanisms for generating suprathermal electrons at the plasmapause/plasmasheet boundary, one involving the ring current and the other not. This in turn raises serious question as to whether the ring current energy is really directly transferred into the SAR arc, whether the process is indirect, or whether there is not even a causal relationship.

For this study, the geomagnetic storm of March 1-4, 1982 was used. A preliminary account of the characteristics of this storm has been given in [9], using BULGARIA-1300 data. Further coincidences with DE-2 during other storms were sought for comparison; for the only case found, the two satellites were in conjugate hemispheres.

Observations

The D_{st} level during the period of the storm is shown in Fig. 1. The sudden commencement occured at about 12.00 h on March 1, and D_{st} reached a level of -215 nT at 06.00 h on March 2. In the same figure, the times of the passes of BULGARIA-1300 and DE-2 passes are shown, identified by their orbit numbers. Relevant data from five BULGARIA-1300 passes were obtained during the storm.

The first is shown in Fig. 2 as orbit 2920 on March 2,1982 at 03:12 UT, three hours before D_{st} reached its maximum extent, and consists of the optical data for the atomic oxygen emissions at 5577 Å and 6300 Å, and the N_2^+ (0,1) band at 4278 Å. The nighttime auroral oval pattern is not very different from that at low activity levels, apart from an increase in the emission rate and an expansion both poleward and equatorward. The terminology for the structure of the auroral oval has been reviewed in [3], and has been further interpreted in terms of spectral ratios. We follow that description and termino logy here. Starting at the poleward limit at the beginning of the pass, there exists until 03:11:45 UT a soft precipitation region, poleward of the oval, dominated by 6300 Å emission called further on the "soft poleward border" Then, the poleward boundary of the oval is crossed, and the discrete component of the oval is entered, extending to 03:14:40 UT and characterized normally by near equality between the 5577 Å and 6300 Å emissions, with a much weaker 4278 Å emission and structured peaks. In this orbit the 6300 Å emission is significantly stronger than 5577 Å emission. Moving equatorwards from 03: 14:40, the diffuse component of the oval is entered; characterized by dominant 5577 Å emission, and near equality between the 6300 Å and 4278 Å emissions. The equatorward boundary of the oval is defined as the point where the 5577 Å emission falls to the level of the 6300 Å emission; it is well defined at 03:16:45 UT, beyond which there is a soft precipitation region equatorward of the oval, called the "soft equatorward border". This region is characterized

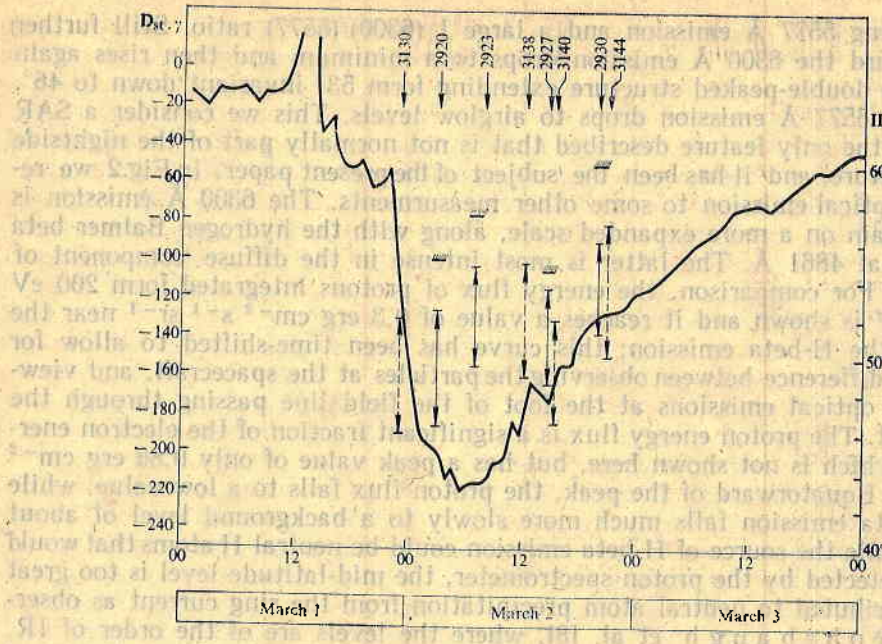

Fig. 1. D_{st} variation during the March 1-4, 1982 storm
The horizontal bars with shaded area represent the equatorial boundary of the oval (1 KeV EBO); full and dashed arrows — the location of SAR arc and suprathermal (st) electrons respectively. Orbit numbers of BULGARIA-1300 and DE-2 satellites indicate the moments of measurement

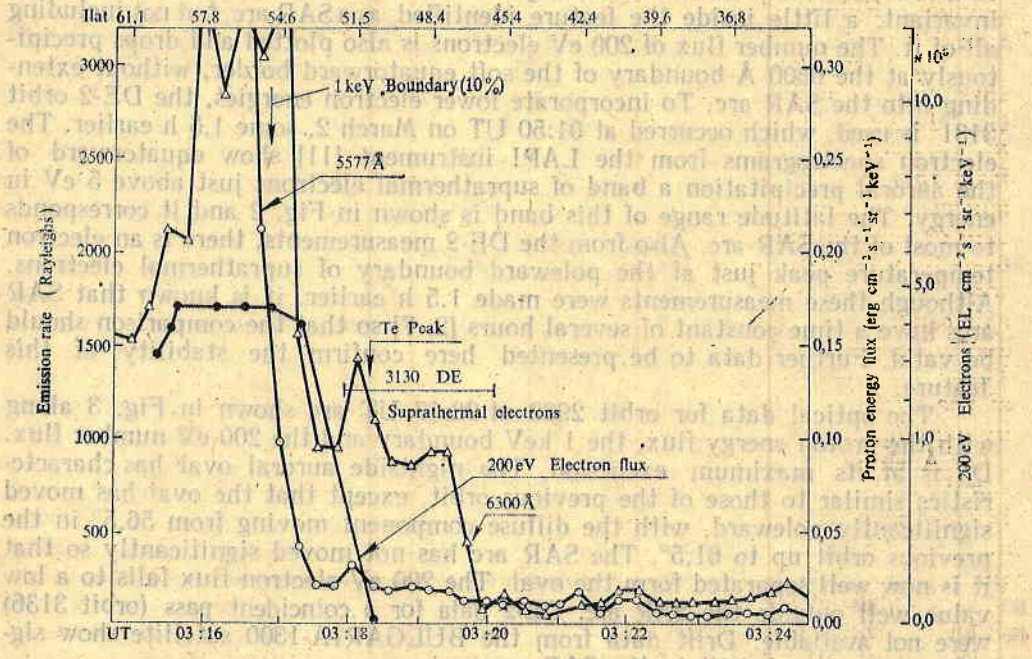

Fig.2. Emission intensities of 6300 Å and 5577 Å along with 200 eV electron flux intensity measured on BULGARIA-1300 orbit 2920
1 KeV EBO is marked by an arrow, as well as the location of suprathermal (st) electrons measured on DE orbit 3130. Invariant latitude (Ilat) is given on top of the figure

by a falling 5577 Å emission and a large I (6300)/(5577) ratio. Still further equatorward the 6300 Å emission drops to a minimum and then rises again to form a double-peaked structure extending form 53° invariant down to 46°, while the 5577 Å emission drops to airglow levels. This we consider a SAR arc; it is the only feature described that is not normally part of the nightside oval structure, and it has been the subject of the present paper. In Fig.2 we relate the optical emission to some other measurments. The 6300 Å emission is shown again on a more expanded scale, along with the hydrogen Balmer beta emission at 4861 Å. The latter is most intense in the diffuse component of the oval. For comparison, the energy flux of protons integrated form 200 eV to 15 keV is shown and it reaches a value of 0,3 erg cm^{-2} s^{-1} sr^{-1} near the peak of the H-beta emission; this curve has been time-shifted to allow for the time difference between observing the particles at the spacecraft, and viewing the optical emissions at the foot of the field line passing through the spacecraft. The proton energy flux is a significant fraction of the electron energy flux which is not shown here, but has a peak value of only 0,86 erg cm^{-2} sr^{-1} s^{-1}. Equatorward of the peak, the proton flux falls to a low value, while the H-beta emission falls much more slowly to a background level of about 60 R. While the source of H-beta emission could be neutral H atoms that would not be detected by the proton spectrometer, the mid-latitude level is too great to be attributed to neutral atom precipitation from the ring current as observed by R o h r b a u g h et al. [8], where the levels are of the order of IR. We conclude that this signal is background from earth-reflected starlight and perhaps artificial sources.

The boundary for 1 keV electrons, defined as the point where the number flux drops to 0,1 of its value in the oval, is also shown. It corresponds to the point where the 5577 Å emission, as shown in the previous figure, has dropped to a low value. The 200 eV boundary, defined in the same way, occurs at 51° invariant, a little inside the feature identified as a SAR arc, but not including all of it. The number flux of 200 eV electrons is also plotted and drops precipitously at the 6300 Å boundary of the soft equatorward border, without extending into the SAR arc. To incorporate lower electron energies, the DE-2 orbit 3131 is used, which occurred at 01:50 UT on March 2, some 1,5 h earlier. The electron spectrograms from the LAPI instrument [11] show equatorward of the auroral precipitation a band of suprathermal electrons just above 5 eV in energy. The latitude range of this band is shown in Fig. 2 and it corresponds to most of the SAR arc. Also from the DE-2 measurements, there is an electron temperature peak just at the poleward boundary of suprathermal electrons. Although these measurements were made 1.5 h earlier, it is known that SAR arcs have a time constant of several hours [2, 7] so that the comparison should be valid. Further data to be presented here confirm the stability of this feature.

The optical data for orbit 2923 at 08:17 UT are shown in Fig. 3 along with the proton energy flux, the 1 keV boundary and the 200 eV number flux. D_{st} is at its maximum excursion. The nightside auroral oval has characteristics similar to those of the previous orbit, except that the oval has moved significantly poleward, with the diffuse component moving from 56,5° in the previous orbit up to 61,5°. The SAR arc has not moved significantly so that it is now well separated form the oval. The 200 eV electron flux falls to a low value well outside the SAR arc. DE-2 data for a coincident pass (orbit 3136) were not available. Drift data from the BULGARIA-1300 satellite show significant westward drift in the SAR arc region.

The next pass, orbit 2927 at 15:04 UT, is shown in Fig. 4. The oval has moved equatorward again to a location similar to that of orbit 2920. The 200

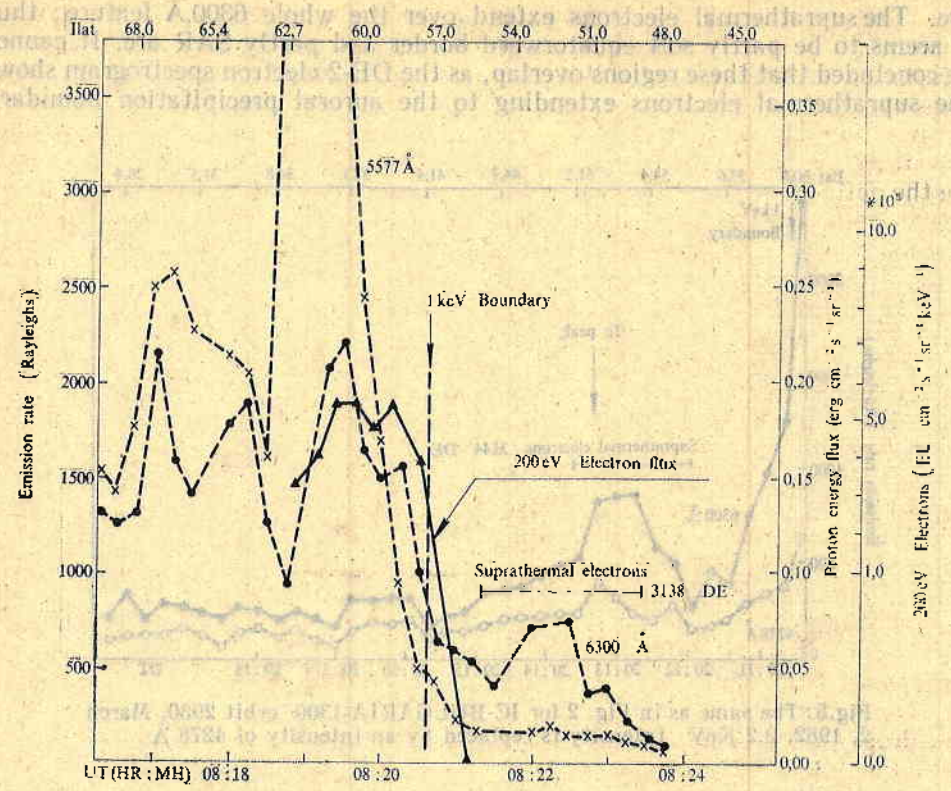

Fig.3. The same as in Fig. 2 for BULGARIA-1300 orbit 2923, March 2, 1982

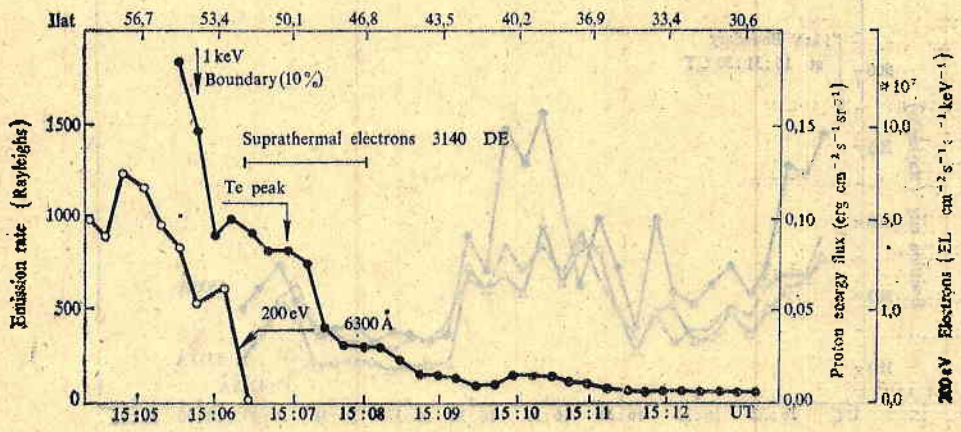

Fig. 4. The same as in Fig. 2 for BULGARIA-1300 orbit 2927, March 2, 1982

eV electons overlap the SAR arc like shoulder of 6300 Å emission, but do not underlie all of it. DE data from orbit 3140, obtained half an hour later show an electron temperature peak extending throughout the whole 6300 Å feature, but perhaps peaking in the equatorward part that we identify with the SAR

arc. The suprathermal electrons extend over the whole 6300 Å feature; thus it seems to be partly soft equatorward border and partly SAR arc. It cannot be concluded that these regions overlap, as the DE-2 electron spectrogram shows the suprathermal electrons extending to the auroral precipitation boundary

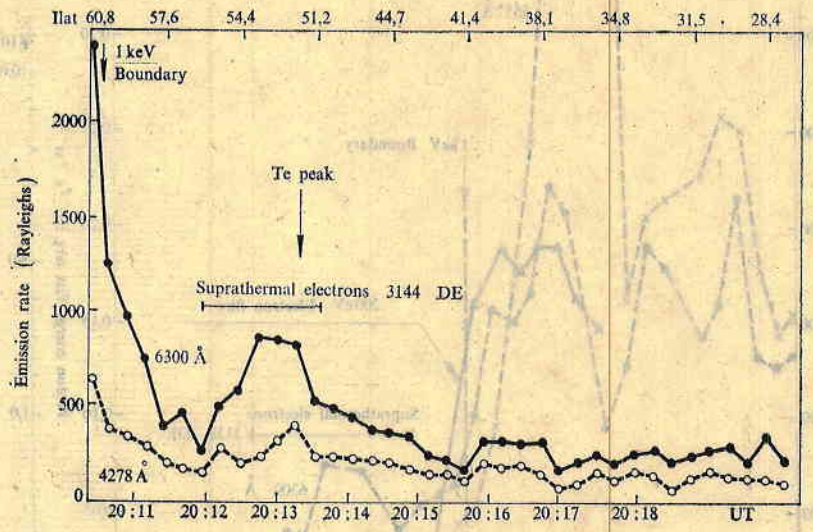

Fig.5. The same as in Fig. 2 for IC-BULGARIA-1300 orbit 2930, March 2, 1982. 0.2 KeV intensity is replaced by an intensity of 4278 Å

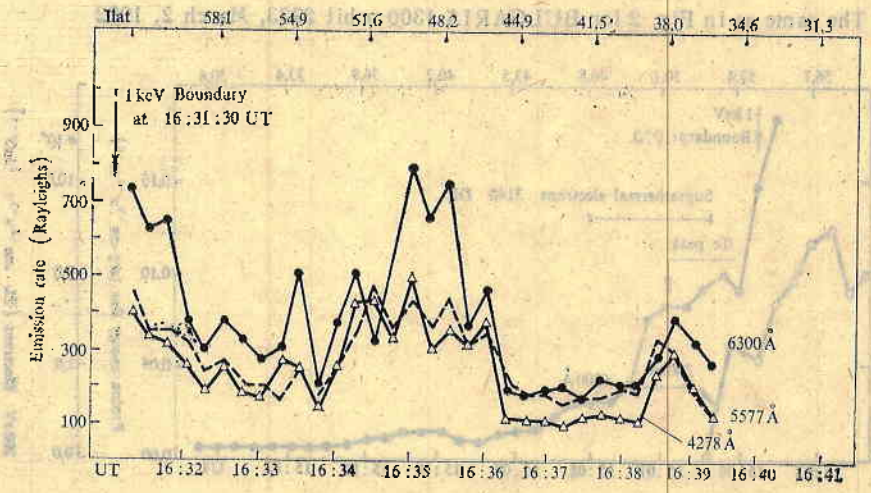

Fig. 6. The same as in Fig. 5 for IC-BULGARIA-1300 orbit 2942

where they become overlaid or replaced by auroral electrons. The strong westward flow observed for the SAR arc region in the previous orbit continues here. Figure 5 shows the data from orbit 2930 at 20:10 on March 2. The auroral oval has moved poleward of 60° invariant and occurs before the start of the pass.

The SAR arc, still located at 53°, is well separated from the oval and is clearly well equatorward of the 200-eV electrons. DE orbit 3155, just 20 min later, displays both the electron temperature peak and the suprathermal electrons that confirm the identification as a SAR arc. The westward flow of the pre-

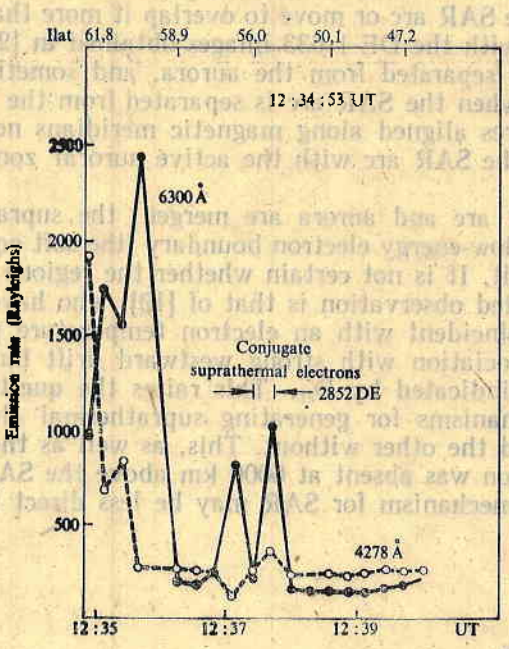

Fig. 7. 6300 Å and 4278 Å intensities on BULGARIA-1300 orbit 2657, February 11, 1982. The double peak enhancement of 6300 Å is compared with conjugate suprathermal electrons on DE orbit 2852 measured in the conjugated ionosphere

vious orbit has ceased, however. The separation of the SAR arc form the oval continues in orbit 2942, at 16:33 on March 3, as shown in Fig. 6. D_{st} has now almost recovered its original level, at -60 nT. Nevertheless, the SAR arc is still present, though slightly weaker than before, at 500 R above background, as compared with 700 R in the previous orbit and about 1 kR during the main phase of the storm.

Finally, we consider for comparison BULGARIA-1300 orbit 2657 for Feb. 11, 1982 at 12:34:53 UT, for which the plot of optical emission is shown in Fig. 7. There appears to be a SAR arc, well separated from the oval, although it is curiously bifurcated. DE-2 orbit 2852 at 11:50 UT was in the southern hemisphere, showing a weak flux of suprathermal electrons located close to one of the two peaks. An electron temperature peak coincides with this, but it is only 2500° K, which would not produce an 800 R SAR arc; this is consistent with the weak flux of suprathermal electrons. In other words, the SAR arc emission in the northern hemisphere is coincident in space but compatible in intensity with the plasma characteristics in the southern hemisphere. This is consistent with the observation presented in [4] that low energy photoelectrons from one hemisphere were blocked from reaching the other hemisphere just in the location of the SAR arc.

Discussion

During a geomagnetic storm, the location of the SAR arc remains remarkably constant near the 53° invariant, while the equatorward auroral boundary may move away from the SAR arc or move to overlap it more than once during the event. This agrees with the DE-1 633 images obtained in [2], which show the SAR arc sometimes separated from the aurora, and sometimes merged with it. However, even when the SAR arc is separated from the aurora, they note that "arc-like features aligned along magnetic meridians near local midnight appear to connect the SAR arc with the active auroral zone several degrees poleward".

When the SAR arc and aurora are merged, the suprathermal electrons extend right to the low-energy electron boundary (the soft equatorward border) and disappear into it. It is not certain whether the regions overlap or simply contact. An associated observation is that of [10], who have observed suprathermal electrons coincident with an electron temperature peak and an electron trough, in association with strong westward drift but without a main phase ring current indicated by D_{st}. This raises the question as to whether there are two mechanisms for generating suprathermal electrons: one from the ring current and the other without. This, as well as the observation that the heated population was absent at 6000 km above the SAR arc [4] suggests that the excitation mechanism for SAR may be less direct than currently believed.

References

1. Cole, K. D. Stable auroral red arcs, sinks for energy of D_{st} main phase. — J. Geophys. Res., 70, 1965, 1689.
2. Craven, J. D., L. A. Frank, K. L. Ackerson. Global observation of a SAR arc. — Geophys. Res. Lett., 9, 1982, 961.
3. Feldstein, Y. I., Yu. I. Galperin. The auroral luminosity and relationship to the large-scale structure of the Earth's magnetosphere. — Revs. Geophys., November, 1985.
4. Gurgiolo, C., D. W. Slater, J. D. Winningham, J. L. Burch. Observations of a heated electron population associated with the 6300 Å SAR arc emission. — Geophys. Res. Lett., 9, 1982, 965.
5. Kozyra, J. U., T. E. Cravens, A. F. Nagy, M. O. Chandler, L. H. Brace, N. C. Maynard, D. W. Slater, B. A. Emery, S. D. Shawhan. Characteristics of a stable auroral red arc event. — Geophys. Res. Lett., 9, 1982, 973.
6. Kutiev I., Electric field generated by the ring current at the plasmapause region. — Adv. Space Res., 1988 (in press).
7. Rees, M. H., R. G. Roble. Observations and theory of the formation of stable auroral red arcs. — Revs. Geophys. Space Phys., 13, 1975, 201.
8. Rohrbaugh, R. P., B. A. Tinsley, H. Rassoul, Y. Sahai, N. R. Teixeira, R. G. Tull, D. R. Doss, A. L. Cochran, W. D. Cochran, E. S. Barker. Observations of optical emissions from precipitation of energetic neutral atoms and ions from the ring current. — J. Geophys. Res., 88, 1983, 6317.
9. Serafimov, K., I. Kutiev. Contribution of Intercosmos — Bulgaria-1300 satellite: Large-scale structure and dynamics of the polar ionosphere during geomagnetic storms. — Results of the ARCAD project and of the recent programmes in magnetospheric and ionospheric physics. Toulouse 84, Centre National D'etudes Spatiales, 1985.
10. Shepherd, G. G., Ts. Gogosheva, M. M. Gogoshev, M. G. Gerdjikova, I. Mendev. Structure and excitation processes in the

nightside auroral oval as observed with the Intercosmos-Bulgaria-1300 satellite. — Planet. Space Sci., 1986 (in preparation).
11. Gogoshev, M., V. Guineva, P. Maglova, T. Markova. SAR-arcs and emissions in the main trough of the electron concentration. — Adv. Space Res., 7, 1987, № 8, 15.

Оптические эмиссии в ночной субавроральной области во время мартовской бури 1—4 марта 1982 г.

Г. Г. Шепард, И. С. Кутиев

(Р е з ю м е)

Во время геомагнитной бури 1—4 марта 1982 г. на нескольких орбитах спутника „Интеркосмос — Болгария — 1300" наблюдалась стабильная авроральная красная (SAR) дуга. По эмиссии 6300 Å видно, что эта дуга иногда находится в контакте с авроральным овалом, а в других случаях — отдельно от него. Когда SAR-дуги перекрываются с овалом, высыпающиеся 200 eV электроны, измеренные спутником, позволяют отделить добавку легких электронов в экваториальной части овала. Часть SAR-дуги экваториально от овала сопровождается присутствием сверхтепловых электронов, наблюдаемых спутниками DE — 2. В работе показано, что сверхтепловые электроны и направленный на запад дрейф могут появиться как во время геомагнитных возмущений, так и в спокойных условиях.

Bulgarian Academy of Sciences

Space Research in Bulgaria, 6
Sofia . 1990

Effects of the topside ionosphere on radiowaves propagation from space objects

*Kiril B. Serafimov, Margarita K. Serafimova**

Central Laboratory of Higher Geodesy, Bulgarian Academy of Sciences
**Geophysical Institute, Bulgarian Academy of Sciences*

The presence of artificial bodies in the outer space calls for a more accurate and strict treatment of problems concerning the radiocommunications with them. Irrespective of the numerous fragmentary studies (see for example our studies [1, 2, 3], as well as of their generalizations in monographs [4, 5, 6, 7]), the notions of the ionosphere used so far are inadequate and not precise enough. The formation of the International Reference Ionosphere (IRI) provided the background for global and precise specification of ionospheric parameters and of their impact on radiocommunications with satellites, rockets, orbital stations, interplanetary stations and other space platforms. Irrespective of a number of deviations from reality and the requirement for IRI perfection [8, 9], we have already got an analytical model for planetary calculations of radio networks and radio ways with space objects. This makes it possible to obtain more accurate analytical expressions and output data for the purposes of telemetry, telecontrol, information transfer and other communications with space aircraft. On the other hand, the reception of natural space radio signals, both for the purposes of radioastronomy and for ionospheric studies (e. g. for the absorption of space radio noise after A2 method), also requires good knowledge of the dependences between radiowaves parameters and those of the propagation medium. Finally, the reception of artificial radio signals from space objects for ionospheric studies (e. g. for Doppler's effect or for Faraday's fading) requires analytical expressions adequate to the real ionospheric effects.

Of all atmospheric parts, the topside ionosphere is the most difficult medium as far as analyses are concerned at least. For at $h > h_mF$ (where h_mF is the height of the maximum electron concentration N_mF or N_mF_2), there are no data available of the hundreds of ionospheric stations and other research equipment covering the Earth. Therefore, when space radio ways and networks are designed, and when research problems are solved, it is more common to use literature data for the topside ionosphere, while for other ionospheric areas the direct results of vertical ionospheric sounding can be ap-

plied. This requires even greater development, improvement and use of IRI references, which is also the subject of this work.

As a considerable part of the multifarious effects of the topside ionosphere on the parameters of radiowaves for space purposes propagating in it have been treated on IRI basis [19, 10, 11, 12, 13, 14, 15] and some other works, we are going to restrict our attention here to posing and solving the problems not treated so far with IRI data, and to giving initial and summary information about other published results.

In this work, similarly to [10, 11, 12, 13, 14, 15] and others, we have used IRI formulae in their first variant (IRI-75) for the sake of convenience of the analytical expressions, without committing ourselves, however, to the concrete IRI-75 data, which are to be improved.

The radiowaves passing through the outer ionosphere undergo deviation and retardation of the radio beam, absorption, refraction, frequency changes, polarization variations, attenuations, scintillations and other effects. We are going to present here in brief the effects untreated so far according to IRI-75, and for the studied ones we are going to make the corresponding references.

1. Radiowaves retardation in the ionosphere and virtual distance increase

The ionospheric impact on retardation refraction and on radio signals retardation is closely related to the accuracy of the satellite trajectory measurements and to other telecommunication problems which are discussed in [4, 5, 6, 7, 16], etc. The initial equation for the heightened distance increase Δl_i owing to the beam retardation in the topside ionospheric plasma is given by the expression (compare for example 17):

$$\Delta l_i = -\gamma f^{-2} \int_{h_m}^{h_s} N_e(h)\,dl, \quad \text{(cf. [7])}, \tag{1}$$

where: h_s is the satellite height or the distance to the magnetospheric boundary (if the space object is outside it or if we work with a radioastronomical source); $N_e(h)$ is the ionospheric profile of electron concentration; the linear element from the radiowaves trajectory dl is determined by the expression:

$$dl = (a+h)\,[(a+h)^2 . n^2 - a^2 \sin^2 Z_0 . n_0^2]^{-1/2} dh, \tag{2}$$

where n is the coefficient of radiowave refraction, $a = 6370$ km is the Earth radius; Z_0 is the initial zenith angle of radiation. At $Z_0 < 85^0$, we can put in (2) $n \approx n_0 \approx 1$ [7]. In this case:

$$dl = (a+h)\,[(a+h)^2 - a^2 \sin^2 Z_0]^{-1/2}\, dh. \tag{3}$$

The group retardation determines (with reading of the transfer coefficients: $\gamma = 40,4$, if the electron density is m^{-3}, and the frequency f in Hz) in this case the following extension of the way:

$$\Delta l_i = \gamma f^{-2} \int_{h_m}^{h_s} N_e(h)\,(a+h)\,[(a+h)^2 - a^2 \sin^2 Z_0]^{-1/2}\, dh. \tag{4}$$

For the vertical profile $N_e(h)$ we use in the case of the outer ionosphere, according to IRI-75, the expression:

$$(5)\qquad N_e(h) = N_m F\left[\frac{A_1}{\left(1+\frac{h-h_m}{A_0}\right)A_2} + A_3 \exp\left(-A_4\frac{h-h_m}{A_0}\right)\right],$$

where A_1, A_2, A_3 and A_4 are constant, A_3 and A_4 are expressed by A_1 (so they are not independent), and constant A_2 has two values: $A_2 = 2$ (low solar activity) and $A_2 = 3$ (high solar activity). In accordance with this we will have the respective two cases in the following analysis:

1.1. Low solar activity ($A_2 = 2$)

We have for retardation:

$$(6)\qquad \Delta l_i = \gamma f^{-2}\int_{h_m}^{h_s}\frac{N_e(a+h)\,dh}{\sqrt{(a+h)^2 - a^2\sin^2 Z_0}} = \gamma f^{-2} N_m F(J_1 + J_2).$$

After replacing (5) in (6), and as a result of the corresponding processing and calculations, we obtain for J_1:

$$(7)\qquad J_1 = \frac{A_0^2 A_1}{\sqrt{b^2 - A^2}}\left[\ln 2\,\frac{b^2 - A^2 + bx + \sqrt{(b^2-A^2)(x^2+2bx+b^2-A^2)}}{x}\right.$$

$$\left. + \frac{b\sqrt{x^2+2bx+b^2-A^2}}{x\sqrt{b^2-A^2}} - \frac{b}{b^2-A^2}\ln\frac{b^2-a^2+bx+\sqrt{x^2+2bx+b^2-A^2}}{x}\right]_{x_s = h_s - h_m + A}^{x_m = A_i}$$

Using analytical replacements, we obtain for J_2:

$$(8)\qquad J_2 = A_3\int_{h_m}^{h_s}\frac{(a+h)\exp\left(-A_4\frac{h-h_m}{A_0}\right)dh}{\sqrt{(a+h)^2 - a^2\sin^2 Z_0}}.$$

To solve this integral, we develop the fast-falling exponential function in the numerator in range, we restrict ourselves to the 5 th member of the range (which is quite sufficient), and for J_2 we finally obtain:

$$(9)\quad J_2 = \frac{A_3 A_4}{A_0}\sqrt{q}\left(\frac{A_4^3}{24A_0^3}\left\{q\left[\frac{q}{5} + 2\left(g^2 + \frac{A^2}{3}\right) - gx^3 - g\left(2g^2 + \frac{3}{2}A^2\right)x\right.\right.\right.$$

$$\left. + (A^2+g^2)^2 + 4\Delta^2 g^2\right] - \frac{A_4^2}{6A_0^2}\left[\frac{1}{4}x^3 + \left(\frac{3}{8}\Delta^2 - \frac{3g}{2}\right)x + 3g^2\right] + \frac{A_4}{2A_0}\left[\left(\frac{1}{3}x - d\right)x\right.$$

$$\left. + \frac{2}{3}A^2 + g^2\right] - \frac{1}{2}x - g + \frac{A_0}{A_4} + \left[\frac{gA^2}{\sqrt{g}}\cdot\frac{A_4^3}{24A_0^3}\left(\frac{3}{2}A^2 - 2g^2\right) - \frac{A_4^2}{6A_0^2}\cdot\frac{1}{\sqrt{g}}\right.$$

$$\left.\left.\left. \times\left(\frac{3}{8}A^2 - \frac{5}{2}A^2 g - g^3\right) - \frac{A_4}{2A_0}gA^2 - \frac{A^2}{2}\right]\cdot\ln\left(x+\sqrt{q}\right)\right\}\right)_{x_m = a+h_m}^{x_s = a+h_s}.$$

In (7) and (9) we use the designations: $A = a\sin Z_0$, $b = a + h_m - A_0$ $g = a + h_m$; $q = x^2 - A^2$.

Obviously in (6) there is quite an adequate expression which can be used for making calculations in different cases.

1.2. High solar activity ($A_2 = 3$)

The retardation is also given by the expression (6). The calculations of J_1 are complicated because of the higher power in the denominator of the integral. In this case, for J_1 we finally obtain:

$$(10) \quad J_1 = \frac{A_0^3 A_1}{b^2 - A^2}\left[\left(\frac{1}{x} + \frac{b}{2x^2} - \frac{6b^2}{4x}\right)\sqrt{x^2 + 2bx + b^2 - A^2} - \frac{-b}{\sqrt{b^2 - A^2}}\left(\frac{3b^2}{2(b^2 - A^2)} - \frac{1}{2}\right)\ln 2 \times \frac{b^2 - A^2 + bx + \sqrt{(x^2 + 2bx + b^2 - A^2)(b^2 - A^2)}}{x}\right]_{x_s = a + h_s}^{x_m = a + h_m}.$$

For J_2, we have expression (9) in this case.

Therefore, at high solar activity we also have sufficiently accurate expressions for the electromagnetic package retardation and the virtual radiowave way extension. Conversely, from the expressions for Δl_i some ionospheric parameters can be found at known retardations and extensions. N_mF is the easiest to determine. Possibilities exist for calculating h_mF and A_0 and A_1 coefficients as well.

2. Refraction of radiowaves passing through the outer ionosphere

The refraction of radiowaves passing through the ionosphere is determined by the expression (compare [7, 17, 18], etc.):

$$(11) \quad \xi_i = -\gamma f^{-2} N_m F(a + h_D) \sin Z_0 \int_{h_D}^{h_s} n^{-1} \frac{dF(h)}{dh} [n^2(a + h)^2 - a^2 \sin^2 Z_0]^{-1/2} dh,$$

where h_D is the initial ionospheric height, and $dF(h)/dh$ is the electron concentration gradient. For the topside ionosphere in the case of the normally used operational frequencies f, which are considerably higher than the critical frequency $f_0F(f_0F_2)$, we can assume that $n \approx 1$ according to [6, 7, 17, 18] and other works. For the medium considered in this case, expression (11) is modified to:

$$(12) \quad \xi_i = -\gamma f^{-2} N_m F(a + h_m) \sin Z_0 \int_{h_m}^{h_s} \frac{dF(h)}{dh} [(a + h)^2 - a^2 \sin^2 Z_0]^{-1/2} dh.$$

In [7] we emphasize precisely the nonpermanent nature of the refraction part in the outer ionosphere, determined with (12). We should like to stress the fact that $dF(h)/dh < 0$ for the outer ionosphere, and for that reason ξ_i is positive for this medium. Thus, certain compensation is reached for the negative refraction in the ionospheric regions with $h \leqq h_m$. We are further going to determine ξ_i using dF/dh distribution according to IRI-75 (see the expression for $N_e(h)$, shown here with formula (5)). Replacing dF/dh from (5) in (12), we obtain:

$$(13) \quad \xi_i = -\gamma f^{-2} N_m F(a + h_m) \sin Z_0 (J_1' + J_2'),$$

where

$$(14)\qquad J_1' = \int_{h_m}^{h_s} \frac{-A_1 A_2 dh}{A_0\left(1+\frac{h-h_m}{A_0}\right)^{2A_2-1}\sqrt{(a+h)^2 - a^2\sin^2 Z_0}};$$

$$(15)\qquad J_2' = -\frac{A_3 A_4}{A_0}\int_{h_m}^{h_s} \frac{\exp\left[-A_4(h-h_m)/A_0\right]dh}{\sqrt{(a+h)^2 - a^2\sin^2 Z_0}}.$$

According to the two values of constant A_2, we have here two subcases as well: at low and at high solar activity.

2.1. Refraction at low solar activity ($A_2 = 2$)

$$(16)\qquad J_1' = \frac{2A_0^2 A_1}{b^2 - A^2}\left\{\left(-\frac{1}{2x^2} + \frac{3b}{2(b^2-A^2)x}\right)\sqrt{(x+b)^2 - A^2} + \frac{3b^2}{(b^2-A^2)^2} - \frac{1}{2\sqrt{b^2-A^2}}\ln 2\,\frac{b^2 - A^2 + bx + \sqrt{(b^2-A^2)[(x+b)^2 - A^2]}}{x}\right\}_{x_s = h_s - h_m + A_0}^{x_m = A_0}.$$

To find J_2', we develop the exponential subintegral function in the numerator in range, and with sufficient accuracy we restrict ourselves to the first five members. On this basis we finally obtain:

$$(17)\qquad J_2' = -\frac{A_3 A_4}{A_0}(J_{20}' + J_{21}' + J_{22}' + J_{23}' + J_{24}' + \cdots),$$

where:

$$(18)\qquad J_{20}' = \{\ln 2A_0[\sqrt{(A_0 x + h_m + a)^2 - A^2} + A_0 x + (h_m + A)]\}_0^{x_s' = \frac{h_s - h_m}{A_0}};$$

$$(19)\qquad J_{21}' = -\frac{A_4}{A_0}\{\sqrt{(A_0 x + h_m + a)^2 - A^2} - (h_m + A)\ln 2A_0 \times [\sqrt{(A_0 x + h_m + a)^2} - A^2 + A_0 x + (h_m + A)]\}_0^{x_s' = \frac{h_s - h_m}{A_0}};$$

$$(20)\qquad J_{22}' = \frac{A_4^2}{2A_0}\left\{\left(\frac{x}{2} - \frac{3}{2}\frac{h_m + A}{A_0}\right)\sqrt{(A_0 x + h_m + a)^2 - A^2} + \left[\frac{3}{2}(h_m + A)^2 - \frac{(h_m + a)^2 - A^2}{2}\right]\frac{1}{A_0}\ln 2A_0[\sqrt{A_0 x + h_m + a)^2 - A^2} + A_0 x + (h_m + A)]\right\}_0^{x_s'}.$$

$$(21)\qquad J_{23}' = -\frac{A_4^3}{6A_0}\left(\left[\frac{x^3}{3} - \frac{5}{6}\frac{(h_m + A)x}{A_0} + \frac{5}{2}\frac{(h_m + A)^2}{A_0^2} - \frac{2}{3}\frac{(h_m + a)^2 - A^2}{A_0^2}\right]\cdot\sqrt{(A_0 x + h_m + a)^2 - A^2} - \left\{\frac{5}{2}\frac{(h_m + A)^2}{A_0} - \frac{3}{2}\frac{[(h_m + a)^2 - A^2](h_m + A)}{A_0}\right\}\cdot\frac{\ln 2A_0}{A_0}[\sqrt{A_0 x + h_m + a)^2 - A^2} + A_0 x + (h_m + A)]\right)_0^{x_s' = \frac{h_s - h_m}{A_0}}.$$

(22) $$J'_{24} = \frac{A_3}{96A_0^3}\left(x^3\sqrt{(A_0x + h_m + a)^2 - A^2} - \frac{7(h_m + A)}{A_0}\left\{\left[\frac{x^2}{3} - \frac{5}{6}\frac{(h_m + A)x}{A_0}\right.\right.\right.$$
$$+ \frac{5}{4}\frac{h_m + A}{A_0^2} - \frac{2}{3}\frac{(h_m + a)^2 - A^2}{A_0^2} + \frac{3}{8}\frac{(h_m + a)^2 - A^2}{A_0^2}\left.\right] \cdot [x - 3A_0(h_m + A)]$$
$$\times\sqrt{(A_0x + h_m + a)^2 - A^2} - 5\frac{(h_m + A)^3}{2A_0^3} - \frac{3}{2}\frac{[(h_m + a)^2 A^2](h_m + A)}{A_0^3}$$
$$\left.\left.\left. + \frac{3}{2}(h_m + A)^2 - \frac{(h_m + a)^2 - A^2}{2A_0^2}\right\} \cdot \frac{\ln 2A_0}{A_0}[\sqrt{(A_0x + h_m + a)^2 - A^2}\right.\right.$$
$$\left.\left. + A_0x + (h_m + A)]\right)_0^{x_s}.$$

2.2. Refraction at high solar activity ($A_2 = 3$)

From (14) at $A_2 = 3$, we obtain:

(23) $$J''_1 = \left[-\frac{1}{3}\frac{x^3}{\sqrt{x^2 + 2bx + b^2 - A^2}} - \frac{1}{3}(I''_1 + I''_2)\right]_{x_m = A}^{x_s = h_s - h_m + A_0}.$$

(24) $$I''_1 = \frac{1}{b^2 - A^2}\left\{-\frac{1}{x} + \frac{b}{b^2 - A^2} + \frac{[12b^2 - 3(b^2 - A^2)]x}{4(b^2 - A^2)^2} \cdot \frac{1}{\sqrt{x^2 + 2bx + b^2 - A^2}}\right.$$
$$\left. + \frac{3b}{\sqrt{b^2 - A^2}}\ln 2\,\frac{b^2 - A^2 + bx + \sqrt{(b^2 - A^2)(x^2 + 2bx + b^2 - A^2)}}{x}\right\}_{x_m}^{x_s};$$

(25) $$I''_2 = \frac{b}{b^2 - A^2}\left(\left\{-\frac{1}{x^2} + \frac{5b}{x} - \frac{120b^4 - 62(b^2 - A^2)b + 12(b^2 - A^2)}{4(b^2 - A^2)^3}\right.\right.$$
$$\left.\left. - \frac{b[60b^2 - 52(b^2 - A^2)]x}{(b^2 - A^2)^4}\right\}\frac{1}{2\sqrt{x^2 + 2bx + b^2 - A^2}} + \frac{15b^3 - 3(b^2 - A^2)}{2(b^2 - A^2)}$$
$$\left.\times\frac{1}{\sqrt{b^2 - A^2}}\ln 2\,\frac{b^2 - A^2 + bx + \sqrt{(b^2 - A^2)(x^2 + 2bx + b^2 - A^2)}}{x}\right)_{x_m = A}^{x_s = h_s - h_m + A_0}.$$

The second part J'_2 is the same at low and high solar activity. Hence, the expressions (17, 18, 19, 20, 21, 22) will be used for J'_2.

The diurnal, seasonal and cyclic variations of refraction are determined by the corresponding variations of $N_mF(N_mF_2)$, the height h_m and the changes of A_0 and A_1. The additional irregular fluctuations of ξ_i depend on the heterogeneities in the electron concentration. We shall consider the effects of heterogeneities in more detail in another part of this work. We should stress, however, the fact that refraction is more strongly affected by these heterogeneities, because usually in their boundary regions there are strongly pronounced local dF/dh gradients. For that reason, the effects of heterogeneities on refraction should not be restricted merely to an analysis of differences in electron concentration $\Delta N_e = N_{\text{novm}} - N_{\text{inhom}}$ in the normal and heterogenous structure, but should be concentrated on the boundary region of dispersion or condensation of the plasma, where the gradient is very high.

The variations of dN_e/dh gradient in different cases, including these from IRI data, have been considered in [19]. It follows from this work that the height h_e of which dF/dh has a maximum, is very close to h_mF. Hence, the

supramaximum region about h_mF has the most essential contribution to refraction. An area with rapid and nonoriented changes of dF/dh has been observed in the region of about $h \approx 600$ km according to rocket data from the VERTICAL series. This region additionally increases refraction.

3. Radiowaves absorption in the topside ionosphere

The radiowaves absorption in the topside ionosphere with $N_e(h)$ distribution according to IRI has been considered in our work [20]. In this work, complete and exact expressions are deduced for the nondeviating absorption at low and high solar activity over middle geographical latitudes. The limiting condition for middle latitudes is required because of the use of linear presentation of the temperature profile $T_e(h)$ with three straight lines in [20], which coincides with the latest IRI variants [21], and is close to the results obtained with the help of the heavy VERTICAL rockets [22, 23]. For the cases of low and high geographical latitudes, the data for ν_{e_i} according to IRI should be used published in [24, 25], and the corresponding data for $N_e(h)$ from IRI.

4. Radiowaves polarization in the topside ionosphere

The polarization losses of radiowaves in the topside ionosphere according to IRI have been presented with the corresponding analytical expressions in [26]. They can be used to calculate the polarization of radiowaves and its equivalent absorption. In [27] a method is shown for IRI adaptation to the concrete data from measurements with a ionospheric satellite and for calculation of polarization losses from the corrected $N_e(h)$ profile. The application of the method to the data from the IC-BULGARIA-1300 satellite has also been demonstrated [27].

5. Topside ionosphere impact on the frequency of radiowaves passing through

The studies of these effects on the basis of the vertical profile $N_e(h)$ according to IRI and present-day data of spatial changes of the Earth's magnetic field, of electron production, the effective neutralization coefficient β_{eff} and the motions in the ionosphere, have been made in [29]. The standard variations of frequency deviations at temporary diurnal, seasonal and cyclic changes of $N_e(h)$ and the other values determining the frequency have also been studied in the same work.

6. Fluctuations of the radio signals phase during the transition through the topside ionosphere

So far there are no generally accepted references of the heterogenous structure of the ionosphere in IRI. For that reason, in [29] on the basis of some materials presented at the COSPAR PANEL and URSI about IRI, and proceeding from the information obtained from INTERCOSMOS-2, 8, 12, 14, 19 and IC-BULGARIA-1300 satellites, some averaged data have been obtained about the fluctuations of different radio signals during their transition in the topside ionosphere.

7. Conclusions and inferences

The expressions obtained here for refraction, retardation and virtual extension of radiowaves way from and to space objects directly solve the problem of the respective effects of the topside ionosphere on radiowaves propagation, a problem not sufficiently tackled so far. Thus a basis is created for an adequate use of IRI in present-day calculations of radio ways and networks. There is a possibility to use the formulae obtained so far for calculating the reverse problem of finding some ionospheric parameters with respectively measured refractions or radiowaves retardations.

We generalized the information about the topside ionosphere impact according to IRI on the propagation of radiowaves passing through (absorption, polarization, frequency deviations, phase fluctuations, etc.) by pointing out the respective sources. Thus, a basis of background data is created for complete use of IRI in studies of radiowaves transition through the topside ionosphere.

References

1. Serafimov, K. On the maximal frequency in space communications. - Compt. Rend. Acad. Bulg. Sci., 19, 1966, No 7, 599.
2. Serafimov, K. The Influence of the ionosphere of the Earth and other planets on the maximal frequency in space communications. — United Nat. Conf. on the Expl. and Peaceful Uses of Outer Space, Doc. A/Conf. 34/I. A. 4, 1968.
3. Серафимов, К. Перспективи за развитието на международните и национални спътникови съобщения. — ПТТР Съобщения, 12, 1973, 254.
4. Колосов, М. А. Распространение радиоволн в космической связи. М., Связь, 1969.
5. Корсунска, Л. П. Распространение радиоволн в связи с искусственными спутниками Земли. Советское радио, 1971.
6. Серафимов, К., Г. Геичева. Космически радиоелектронни системи. С., Държавно военно издателство. 1973.
7. Яковлев, О. И. Распространение радиоволн в Космосе. М., Наука. 1985.
8. Rawer, K., C. Minnis, K. Serafimov. Towards an Improved International Reference Ionosphere. — Adv. in Space Res., 4, No 1, 1984.
9. Серафимов, К. Международната референтна йоносфера и радиосъобщенията. — Радио, телевизия и електроника, 34, 1985, № 2.
10. Serafimov, K. Adaptability of N(h)-profile by model IRI to measurements of coherent frequences. — Compt. Rend. Acad. Bulg. Sci., 32, 1979, No 12, 1651.
11. Serafimov, K., M. Gogoshev, B. Taneva, Ts. Gogosheva, I. Mendev, Z. Pashova. Adaptation of International Reference Ionosphere to combined ground and satellite measurements. — Compt. Rend. Acad. Bulg. Sci., 32, 1979, No 10, 1343.
12. Serafimov, K. Determination of model vertical distribution of electron temperatures and concentration by satellite and ground-based measurements. — Compt. Rend. Acad. Bulg. Sci., 33, 1980, No 2, 199.
13. Serafimov, K. Some measurements possibilities for the improvement of IRI. — Adv. in Space Res., 4, 1984, No 1, 133.
14. Serafimov, K., S. Spassov, G. Georgiev. Improvement of the electron density distribution in the outer ionosphere, according to IRI, with measurements of natural optical emissions. — Bulgarian Geophys. Journal, 10, 1984, No 3, 10.
15. Hoang, L., K. Serafimov, I. Kutiev, M. Karadimov. Bottomside N(h) profiles over Vietnam and their comparison with IRI. — Adv. in Space Res., 4, 1984, No 1, 65.
16. Le Vine, D. M., Propagation delay in the atmosphere. — Radio Sci., 7, 1972, No 6, 625.
17. Titherigge, I. E. The refraction of satellite signals. — Journ. Atm. Terr. Phys., 26, 1964, No 2, 531.
18. Воронин, А. Л. О рефракции радиоволн в ультракоротком диапазоне в йоносфере. — Геомагнетизм и аэрономия, 4, 1964, № 3, 531.

19. Serafimov, K. On the formation of structure of topside ionosphere. — Compt. Rend. Acad. Bulg. Sci., 39, 1986.
20. Serafimova, M., K. Serafimov. The absorption in topside ionosphere by data of IRI. — Compt. Rend. Acad. Bulg. Sci., 39, 1986.
21. Bilitza, D. Improved analytical representation of electron temperature in the IRI. — Adv. in Space Res., 4, 1984, No 1, 93.
22. Serafimov, K., I. Kutiev. Approximation for electron temperature distribution by vertical rocket data. — Compt. Rend. Acad. Bulg. Sci., 32, 1979, No 1, 31.
23. Серафимов, К. Космические исследования в Болгарии. С., БАН, 1979.
24. Serafimov, K., I. Kutiev, M. Serafimova. Electron-ion collision frequency in ionosphere. — Compt. Rend. Acad. Bulg. Sci., 39, 1986.
25. Serafimov, K., I. Kutiev, M. Serafimova. Collision Frequency in the Ionosphere by IRI. BAS, S., 1986.
26. Serafimov, K. Polarization losses of radiosignals in the ionosphere in agreement with IRI. — Bulgarian Geophysical Journal, 10, 1984, No 2, 23.
27. Serafimova, M. Telecommunications and the Satellite "Intercosmos-Bulgaria-1300" — IAF-83-09, 34 Congress of IAF, Budapest, Edited by AIAA, NY, 1983.
28. Серафимов, К., М. Серафимова. Въздействие на външната йоносфера върху честотата на преминаващите през нея радиовълни. — Бълг. геофиз. списание, 12, 1986, № 4.
29. Serafimova, M., K. Serafimov. On the fluctuation of radiosignals in topside ionosphere. — Compt. Rend. Acad. Bulg. Sci. (in print).

Воздействия внешней ионосферы на распространение радиоволн из космических объектов

К. Б. Серафимов, М. К. Серафимова

(Резюме)

Проанализированы основные воздействия внешней ионосферы на проходящие через нее радиоволны. На основе Международной референтной ионосферы получены выражения для: а) запаздывания радиоволн и виртуального увеличения расстояния их распространения; б) рефракции радиоволн; в) поглощения; г) флюктуации фаз радиосигналов при переходе через внешнюю ионосферу. Сделан анализ условий нижней и высокой солнечной активности. Даются рациональные рекомендации и подводятся исходные зависимости. Даются рациональные рекомендации для определения основных параметров радиосвязи с космическими объектами.

Bulgarian Academy of Sciences

Space Research in Bulgaria, 6

Sofia . 1990

On self-similar solutions in disc accretion problems

Lachezar G. Filipov

Space Research Institute, Bulgarian Academy of Sciences

The theory of disc accretion has recently become an important factor for the solution of many astrophysical problems. Accretion discs are considered to play a major role in the modelling of quasars, nuclear active galaxies and X-ray sources in narrow binary stars. We have enough grounds to claim that the structure of stationary thin accretion gas discs is relatively well studied [15].

Regardless of the progress in these studies, the fundamental problem of the disc accretion theory, i. e. of its viscosity nature, is still to be resolved. Obviously, theoretical investigations are not sufficient. Regular observation data should be used on a broader scale accompanied by comparisons between theoretical models and experimental results.

The non-stationary disc accretion is defined in many cases, where discs are assumed to exist or are observed in the studied objects. Therefore, the investigation of this type of solutions will present the basis of understanding the natural physical phenomena and processes. The study of non-stationary discs provides possibility to make scientifically justified conclusions about the nature of the viscous mechanisms responsible for the transport of the motion quantity momentum in the discs.

Many publications on non-stationary disc accretion are devoted to these problems [8, 9, 10, 11, 12, 13].

In another publication of ours we have found out that the temporal behaviour of thin accretion discs may be described with the non-linear differential maintainance of "diffusion":

$$\frac{\partial F}{\partial t} = A\frac{F^m}{h^n}\frac{\partial^2 F}{\partial h^2}, \tag{1}$$

where h is the specific angular momentum and F is the friction momentum between two adjacent cylindrical layers in the disc [12]; the parameters m and n are determined by the viscosity nature and the opacity law of the disc [10]. A is a "diffusion" coefficient determining the velocity of the processes.

A non-linear diffusion equation of a simpler type has particular invariant self-similar solutions. It is known that the idea of self-similarity is related to

the transformation groups [1, 3, 4, 5, 7]. These transformations are represented into the differential or the integrodifferential equations of the process. The group of transformations for the given equation is determined by the dimensions of its input values: time reference unit, length, mass, etc., which represent a simple case.

This type of self-similar solutions is featured with power indices, which represent simple quotients, determined elementary by dimensional analysis operations and known as first order solutions.

We shall define further the role of these self-similar solutions and shall demonstrate the pattern of their application into viscosity problem solutions. Self-similarity is a phenomenon whose features are obtained at different time moments by the transformation of similarities in sequential order. The scales of similarity, in turn, represent a function of the main physical parameters of the equation describing the physical phenomenon.

Let us examine the temperature diffusion equation for stationary conductive medium:

$$\frac{\partial T}{\partial t} = Q \nabla T,$$

where Q is the constant diffusion, T is the temperature and t is the time. The problem is to determine the temperature in the successive moments, if the initial distribution is $T = Br^{\beta}$, where r is the distance to the centre of the coordinate system. If we define the scale of the temperature θ, the distance L and the time τ then we can determine dimensions Q and B: $[Q] = \tau^{-1}L^2$ and $[B] = L^{-\beta}\theta$.

Q is the only constant independent of θ. The problem is precisely determined and there is no other constant of length or time dimension to be obtained from the elements given above. Therefore, such a constant should not be present in the solution. Sometimes, after the beginning of the process, the typical length scale depending on the time may be defined as:

$$L_c(t) = (Qt)^{1/2}.$$

The time-dependent temperature scale may be defined in a similar way:

$$T_c(t) = BL_c(t)^{\beta}.$$

The solution of the problem should yield T as a function of t and r. In non-dimensional form this is:

$$\frac{T}{T_c} = \frac{T}{BL^{\beta}}.$$

The non-dimensional form should be a function of $\frac{r}{L_c(t)}$ and $\frac{t}{t}$. The latter is naturally a zero and does not enter the examined problem since t is measured in $[\tau]$ alone and may be expressed by Q, B and t. Thus, we obtain the solution in the form of $T = BL_c^{\beta}T_*\left(\frac{r}{L_c(t)}\right)$, where $L_c(t)$ is already defined and T_* is a non-dimensional function composed of its non-dimensional arguments. The obtained result is a self-similar solution, since time-dependent scales are used. The temperature scale is always a function of the scale featuring length. It is the self-similarity of the problem which denotes that variable scales of L_c and T_c may be selected, which provides for the possibility to represent the scale of the phenomenon characteristics by a single variable function.

Therefore, the presence of several dimensions of the independent constants, including the boundary conditions of the problem, defines the necessity of a self-similar solution.

Let us examine now several problems where the self-similar solutions are of first order [1,3]. The first problem — the time behaviour of a thin disc — is determined by equation (1) under the assumption that for the initial momentum $t=0$ the distribution is:

$$F = Bh^{\alpha}. \tag{2}$$

The dimensions of all values in equation (1) and the initial condition (2) are:

$$[h] = L^{2}\tau^{-1}; \quad [t] = \tau; \quad [F] = ML^{2}\tau^{-2};$$
$$[A] = M^{-m}L^{-2(n-m+2)}\tau^{2n-m-3}; \tag{3}$$
$$[B] = ML^{2(1-\alpha)}\tau^{\alpha-2},$$

where τ is the time dimension, M is the mass dimension and L is the length dimension.

Let us determine the typical scale of the total angular momentum $h_c(t)$ and the typical friction momentum scale $F_c(t)$ for each moment $t>0$. The first value is yielded by the dimensional analysis of equation (1), namely:

$$h_c(t) = (AF_c(t)^m t)^{\frac{1}{n+2}}, \tag{4}$$

and for $F_c(t)$ we use the initial distribution:

$$F_c(t) = Bh_c(t)^{\alpha}. \tag{5}$$

Substituting expression (5) into (4), we obtain for h_c:

$$h_c(t) = (AB^m t)^{\frac{1}{n+2-\beta m}}. \tag{6}$$

The solution of the problem yields F as a function of h and t and may be written down in a non-dimensional form as:

$$\frac{F}{F_c} = \frac{F}{Bh_c(t)^{\alpha}} = F_*\left(\frac{h}{h_c}, \frac{t}{t}\right) = F_*\left(\frac{h}{h_c}\right).$$

Therefore, the function F will take the shape of:

$$F(h,t) = Bh_c^{\alpha}(t)F_*\left(\frac{h}{h_c}\right). \tag{7}$$

If we substitute (6) into (7), we shall obtain the dependence in developed form, and using equations (7) and (1) we may write the following equation for F_*:

$$\left(\frac{\alpha}{n+2-\alpha m}\right)F_* - \left(\frac{1}{n+2-\alpha m}\right)\xi\frac{dF_*}{d\xi} = \varphi(t)\frac{F_*^m}{\xi^n}\frac{d^2F_*}{d\xi^2},$$

where $\xi = \frac{h}{h_c(t)}$. The function $\varphi(t)$ is an expression containing only the time. This function should equal a unit in order to provide a self-similar solution

for the above equation. And, indeed, for each distribution of the type (2) this condition is satisfied. Therefore, we may write down equation (8) in the final form of:

$$(8)\qquad \left(\frac{\alpha}{n+2-\alpha m}\right)F_* - \left(\frac{1}{n-2-\alpha m}\right)\xi\frac{dF_*}{d\xi} = \frac{F_*}{\xi^m}\frac{d^2F_*}{d\xi^2}.$$

Equation (8) provides the possibility for both qualitative and quantitative description of some non-stationary phenomena in the accretion disc. This feature of equation (8) has been the subject of our other works [10].

The second problem leading to a self-similar solution of first order for equation (1) is the following: the evolution of the accretion disc is described by equation (1) under the condition that the time development of the initial configuration is satisfied throughout the process by the integral of the total substance angular momentum [2], namely:

$$(9)\qquad K = 2\pi\int_{r'}^{r''}\Sigma' hrdr,$$

where Σ is the surface disc density [15], h is the angular momentum and r is the distance to the disc center. Substituting Σ with F similar to the procedure in equation (1) [10], we obtain the following condition:

$$(10)\qquad K = 2\pi\int_{h'}^{h''}F^{1-m}h^{1+n}dh = \text{const}.$$

Another approach to find the necessary conditions for the availability of self-similar solution of equation (7) is to determine the power indices α and β in solutions of the type:

$$(11)\qquad F = Ct^{-\alpha}F_*(\xi),$$

where $\xi = \frac{h}{Bt^{\beta}}$,

which reduces the problem to a routine differential equation of finite conditions.

After substituting equation (11) into (1) and (10), we obtain the following necessary conditions for the availability of a self-similar solution:

$$(12a)\qquad \alpha = 1,\quad \beta = \frac{1-m}{2+n};$$

$$(12b)\qquad C = \frac{K}{2\pi A}\qquad B = \left[\frac{A^{1-m}K^m}{(2\pi)^m}\right]^{\frac{1}{n+2}}.$$

The equation which defines the function F_* is:

$$(13)\qquad F_*^m\frac{d^2F_*}{d\xi} + \left(\frac{1-m}{2+n}\right)\xi^{n+1}\frac{dF_*}{d\xi} + \xi^nF_* = 0.$$

We shall examine below some possible astrophysical phenomena, where this solution can be applied.

If a stationary disc has existed in a binary system prior to a certain moment, and due to some reason the inflow of the normal component ceases, this solution will describe the evolution of the reminder of the disc substance.

The same approach on the applicability of equation (13) can be made in the following manner: if we have a distribution of the type $F=\Phi(h)$ at the initial moment, then it will contribute indirectly to integral (10). The function $F=\Phi(h)$ should simply be determined with respect to h.

We have to underline here that this method provides a possibility to expand the number of the astrophysical problems, which may be resolved by the first problem set up in this paper, since the substantial fact is that the distribution should represent a power law of the specific angular momentum. The unique condition to be met by the solution of equation (13) is to satisfy the law of preserving the quantity of the total angular momentum throughout the time development of the initial configuration. Of course, the best proof of this affirmation will be to compare the solutions of equations (13) and (1) for particular derivatives.

Another type of this problem relates to the modelling of the substance behaviour in accretion discs, when the mass integral is satisfied during the evolution process.

Let us examine again equation (1). Applying by analogy the method used by Sedov [7] for the obtaining of the mass integral with reference to rotating fluid, we can obtain the corresponding algebraic integral for the solution of our problem.

Following the same pattern, let us examine the demensions of the input values:

$$[F]=ML^2\tau^2;\quad [h]=L^2\tau^{-1};\quad [\Sigma]=ML^{-2};\tag{14}$$
$$[M]=M;\quad [B]=L^3\tau^{1-\delta}.$$

We are looking for a solution of the type $F=Bt^{-\alpha}F_*(\xi)$, where $\xi=\frac{h}{bt^\delta}$.

Following Sedov's approach [7], we introduce a supplementary parameter $[a]=ML^k\tau^s$, where a, k, s are unknown, if no particular consideration on the nature of the phenomenon is involved.

Using in a summarized manner the above mentioned development, we can determine some supplementary values, namely:

(15) a) $v_r=\frac{r}{t}V(\xi)$ radial velocity;

(16) b) $\Sigma=\frac{a}{r^{k+3}t^s}R(\xi)$ surface density;

(17) c) $M=\frac{a}{r^k t^s}M(\xi)$ the mass between two fixed radii.

Performing almost the same computations as in [7], we obtain the mass integral in a final form as:

$$\{(s+2\delta k)M(\xi)-2\pi R(\xi)(V(\xi)-2\delta)\}=\text{const}\,\xi^{2k}.\tag{18}$$

Knowing functions $R(\xi)$ and (ξ), we may determine the temporal mass behaviour between two radii. Using the theory of the disc accretion, these relations take the shape of (14):

$$R(\xi)=\xi^{n+2k+1}F_*(\xi)^{(1-m)};\tag{19}$$

$$V(\xi)=-\xi^{-(n+1)}F_*^{-(1-m)}\frac{df}{d\xi}.\tag{20}$$

The equation satisfying function $f(\xi)$ is similar to equation (13) but the coefficients differ:

$$F_*^m \frac{d^2F_*}{d\xi^2} + \delta\xi^{n+1}\frac{dF_*}{d\xi} + \alpha\xi^n F_* = 0, \tag{21}$$

where α, δ are defined by dimensional analysis.

Let us examine the values v_r and Σ in view of the disc accretion theory, using the dependences which are relevant to each and any moment. Our purpose is to determine the dependence between the dimension coefficients and the power indices. As a final result we obtain the following equation system defining the power indices:

$$\begin{aligned} &2k\delta + s + 1 = 0; \\ &\delta(2k+n+1) - \alpha(1-m) + s = 0; \\ &2k\delta + \delta + 1 - \alpha - s = 0; \\ &2\delta + \delta n + \alpha m - 1 = 0. \end{aligned} \tag{22}$$

The solutions corresponding to the system (22) are:

$$\begin{aligned} &\alpha = -\frac{1}{n+2-m}; \quad \delta = \frac{1}{n+2-m}; \\ &K = \frac{1}{2}(m-n-3); \quad s = \frac{1}{n+2-m}. \end{aligned} \tag{23}$$

Thus, with the power indices obtained and for the finite conditions of the function F_*, the equation (21) yields a solution which describes the temporal behaviour of the accretion disc under the condition that the mass integral is satisfied. The solution of the equation (21) with the power indices (23) may be used for describing the temporal evolution of the substance tore formed around a gravity centre.

In the case where the right-side constant of equation (18) differs from a zero, we shall observe in dependence on the sign either an increase or a decrease of the total tore or disc mass.

We should note that usually in a real time situation both algebraic integrals must be used, i. e. the integral reflecting the situation prior to the moment of quantity motion and the mass integral. When we examine the case of a disc evolution involving contribution of a substance flux inflowing from a secondary component, both the disc mass and the moment of quantity motion change. This imposes the necessity of investigating more complicated problems which will be the subject of further studies.

Discussion

The three methods proposed for the solution of the problems related to equation (1) provide for the possibility of building up both quantitative and qualitative models of non-stationary sources with the assumed existence of accretion discs. The obtaining of a large class of particular solutions and their comparison with the observational data for transient and cataclismic stars provides for the closer understanding of the physical processes of the disc accretion. Examining the methods given here and based on a general analysis approach, as well as comparing them with similar physical methods [1, 4, 5, 7], we can obtain the power index solutions depending on the parameters m and n. In turn, they will provide the definition of the physical processes of the thin accretion disc viscosity and of the plasma opacity.

On the basis of observations of cataclismic stars and transient X-ray sources it is determined that their luminosity after attaining a maximum decreases almost after a power law in time. This provides grounds to believe that by comparing the model solutions and the existing physical hypotheses we can obtain estimation of the scale and nature of the physical processes in the disc.

On the other hand, this paper examines only methods providing for the obtaining of self-similar solutions of first order. Second order soutions are also available [1, 4]. The second order solutions provide for the possibility of estimating new models, thus yielding solutions of this order based on astrophysical considerations.

In conclusion we shall underline another essential fact. Equation (1) is closely approximating the equations describing the combustion processes and some of the plasma processes [6]. Certain non-routine processes, typical for non-linear plasma and combustion properties are also to be observed within these physical phenomena, i. e. self-organization, self-focusing, etc. This provides grounds to believe that such phenomena may also be expected in disc accretion processes. These aspects deserve specific attention and should become the subject of future investigation of the nature and the properties of the accretion discs.

References

1. Баренблатт, Г. И. Подобие, автомодельность, промежуточная асимптотика. Л. Гидрометеоиздат, 1978, p. 206.
2. Богоявленский, О. И. Методы качественной теории динамических систем в астрофизике и газовой динамике. М. Наука, 1980, 320.
3. Дибай, Э. А., С. Л. Каплан. Размерность и подобие астрофизических величин. М. Наука, 1976, 399.
4. Зельдович, Я. Б., Ю. П. Райзнер. Физика ударных волн и высокотемпературных гидродинамических явлений. М. Наука, 1968, 686.
5. Зельдович, Я. Б., А. С. Компанеец. Физико-химическая и релятивистская газодинамика. М. Наука, 1977, 287.
6. Самарский, А. А., С. П. Курдюмов, Н. В. Дмитренко, П. Михайлова. Нелинейные процессы в плотной плазме и особенности термодинамики режимов обострения. Препринт № 109 ИПМ АН СССР, 1976.
7. Седов, Л. И. Методы, пособия и размерности в механике. М. Наука, 1977, 440.
8. Сюняев, Р. А., Н. И. Шакура. Диски-накопители в двойных системах и их наблюдательные проявления. Письма в А. Ж., 3, 1977, 262-266.
9. Bath, G. T., J. E. Pringle. The evolution of viscous disc-mass transfer variation. Mon. Not. Astr. Soc., 194, 1981, 967-986.
10. Filipov, L. G. Self-similar problems of the time-dependent disc accretion and nature of the temporary X-ray sources. Adv. Space Res., 3. 1984, 305-313.
11. Lightman, A. P. Time-dependent accretion disc around compact objects, I. Theory and basic equations, II. Numerical models and instability of inner region. Appl. J., 194, 1974, 419-437.
12. Lynden-Bell, D., J. E. Pringle. The evolution of viscous discs and origin of the nebular variables. Mon. Not. Astr. Soc., 168, 1974, 603-637.
13. Lüst, R. Die Eutwielung einer um einen Zentralkorper rotierenden gasmasse. I Lösungen der hydrodynamischen Gleichungen mit turbulenter Reibung. Z. Naturforsch, 7d, 1952, 87-95.
14. Novikov, I. D., K. S. Thorne. In black holes. Les. Astres., Occlus ed., C. de Witt, B. S. de Witt, N. Y. Gordon S. Breach, 1974.
15. Shakura, N. I., R. A. Sunyaev. Black holes in binary systems. Observational appearance. Astron Astrophys., 24, 1973, 337-355.

Об автомодельных решениях задачи дисковой акреции

Л. Г. Филипов

(Резюме)

Гидродинамические уравнения используются как один из методов моделирования нестационарных дисков вокруг одной из компактных компонентов в двойных системах.

Полученные модельные уравнения — нелинейные и могут быть решены при помощи численных или теоретико-групповых методов.

В настоящей работе автор использует модельное уравнение, исходя из предположения, что законы вязкости и непрозрачности являются степенными функциями локальных параметров акреционного диска.

Данные наблюдения нестационарных компактных объектов, где можно ожидать существования акреционных дисков, сравнивали с решениями уравнений, содержащих большинство общих предположений о физических процессах в дисках. Автор считает, что это найдет применение в определении природы и масштаба явлений. Таким образом сформулированны три реальные астрофизические проблемы, считая, что они ведут к автомодельным решениям первого рода, используя уравнения, полученные в настоящей работе.

Bulgarian Academy of Sciences

Space Research in Bulgaria, 6

Sofia . 1990

A computing programme for coordinate transformations of vector magnetometer data

Alexander Z. Bochev, Stoyan Ts. Hadjistoyanov,, Nikola B. Istatkov*, Hristo M. Georgiev***

Space Research Institute, Bulgarian Academy of Sciences, Sofia
**Research Institute of Organization in Machine Works, Sofia*
***Geophysical Institute, Bulgarian Academy of Sciences, Sofia*

Introduction

The *in situ* measurements of the magnetic field vector with three-component flux-gate magnetometer carried out in the ionospheric-magnetospheric region allow to obtain important information on the electric currents along the field lines of the magnetic field of the Earth, on the ionospheric current systems, and on the main magnetic field and its secular changes. These data are also useful for the solution of other problems — computation of the induced electric field $V \times B$ in reducing electric field measurements representing a portion of complex experiments, in determining the actual orientation, etc.

These problems are resolved with precise measuring magnetometric equipment [1]. Besides, the data processing should also be correct and should facilitate data application in scientific analysis and estimates of the technical state of the measurements during performance and especially during continuous experiments.

Significant advantage of the magnetometric data analysis is the availability of a model of the main Earth magnetic field, and of the field generated in the Earth's interior respectively as, for example, IGRF-1980, GSFC/12/83, etc. This is an important premise for the study of the outer magnetic field, generated by ionospheric-magnetospheric sources [2].

Another premise for this elaboration is the methodics suggested for the coordinate transformations of the magnetometric data provided by a near-earth orbiting satellite [3]. It is assumed that the magnetic disturbances by field-aligned currents in coordinate systems related with an excentric dipole are transformed into two-dimensional, which facilitates their analysis and interpretation.

We can mention, on the other hand, the necessity of connecting the methodics for the determination of the magnetic axes orientation of the sensor with a common software system [4].

The individual aspects of the methodics were specified and supplemented in the process of testing of the developed programmes. The following goals were pursued in obtaining the end software product: reduction of the input-output operations at the expense of increasing the processing rate; decrease of the magnetic tape number; simplification of the usage; analysis of the causes for computer processing interruption, detailed message output on the causes and options of processing continuation from the interruption site.

Description

The general flow chart is shown in Fig. 1. The SEANCE programme is a control module. It drives the modules implementing the individual steps of the technological process. Input data and operation control parameters are supplied to the SEANCE programme. The input data are: magnetic tape with

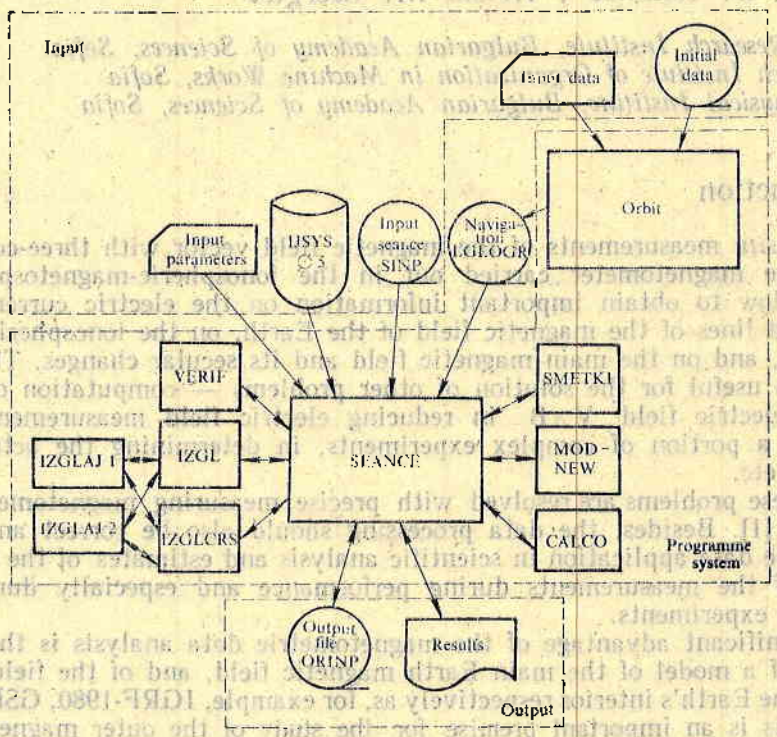

Fig. 1

navigational parameters — LGEOGR; magnetic tape with telemetric data — SINP; disc file with correcting co fficients — IYSYSO 5.

The following data serve to control the software mode of operation with the aid of parametric cards: beginning/end of measurement to ensure proces-

sing of determined seance period. If these parameters are not provided, the complete seance is processed and the beginning/end times are taken from the header block of the telemetric information; format flags of the introduced steps (interval steps of the input seance, step of input band with geography and step of output band); module input parameters — MODNEW.

The software output is a tape file, containing the following information: interval number, time, geographic coordinates, measured components, theoretical components, differences between measured and modelled field in different geophysical coordinate systems, geophysical coordinates of observed points, orientation telemetric data (angular velocities and solar situation). Line printer information of step 8 s is printed simultaneously with the formation of the magnetic tape.

The SEANCE software executes the following steps: stores tables (calibration data) into the main memory; reads the header block of the telemetric information and prints it upon selection; reads the parametric cards and initiates its functions in agreement with the data contained in them; transmits control to MODNEW module, which executes the preparatory steps for the magnetic field model application; reads 190 intervals from the telemetric information. They are tested against uncertainties, i. e. against deviations from the smooth change of the compensation step numbers. This is done by VERIF module. If intervals are reliable we proceed to "smoothing" the telemetric information in order to eliminate deviations at the reswitching of steps. For the purpose, IZGL and IZGLCRS modules are used, which in turn function via the auxilliary modules IZGLAJ 1 and IZGLAJ 2. They reveal step change instances and determine reliable intervals before and after reswitching. Assuming both smoothly changing process and short intermediate process duration — up to 1 sec, the "smoothing" is made with the aid of a straight line across the already determined reliable intervals. The four modules are loaded in order to process cases, where the reswitching is made within the limits of the 190 intervals available in the main memory.

After completing the above mentioned steps, the control is transferred to SMETKI module, which converts the information into physical paremeters. The SEANCE module combines the 190 intervals read into the main memory with the navigation data. The records are compared after measurement time. A special subroutine maintains comparison time of the measurements. This is formed on the basis of the assumption that the time of each sequential interval is obtained form the time of measurement adding a constant step. If due to certain reason the time of the entering interval differs from the comparison time within the limits of half a step, a correction of time is introduced transposing comparison time into the record obtained. A warning message is issued. In this case it is assumed that the difference is the result of random disturbance during the determination of the time of measurement. In case we obtain a greater difference for a given interval, an error message is printed and SEANCE procedure ceases operation in emergency mode.

The so-called "reference points" are formed during the combination between navigation data and output records depending on the step given as input parameter. These are the output records containing navigation data.

The CALCO module for main earth-magnetic field computations (IGRF-1980) is finally included. The field is represented in series by spherical harmonic coefficients. The differences between the measured model field by components and module are also computed. The 190 intervals, combined with navigation data and processed during the former steps, are read as input data. The model of the main magnetic field is computed for the respective geogra-

phic coordinates, located at the reference points. A step of 8 s is selected, containing precise number of intervals. The differences between measured and model field for the intermediate points are obtained with linear interpolation of the model values at the reference points. The CALCO module computes the coordinates of the excentric dipole in earth radii units, the coordinates of the north pole of the excentric dipole, the polar angle and the long. in grades. The same module transforms the geographic lat. and height into geocentric supplement to the lat. and a geocentric radius. The model field is computed into topocentric coordinates and is transformed into geodetic (geographic) coordinates. Coordinate transformations of the observation point are made, i. e. from Cartesian geodetic into Cartesian geomagnetic, spherical geomagnetic, Cartesian excentric geomagnetic, spherical excentric geomagnetic, excentric radius and modified excentric lat. As a result of temporal transformations, we obtain the geomagnetic local time and the excentric geomagnetic time. Afterwards, an interpolation between the reference points is made. For each observation point a transformation is made, i. e. the measured field is converted from orbiting into topocentric coordinate system and further into topocentric geomagnetic, topocentric geomagnetic with one axis along the magnetic field, excentric geomagnetic and excentric geomagnetic with one axis along the magnetic field.

Finally the SEANCE module forms the output records of the magnetic tape from the 190 processed intervals. The described cycle of performance is repeated until the input information for the determined period of processing time is exhausted.

The information on the output magnetic tape can be used for the general case of the geophysical analysis. In case no unifold interpretation is possible, an orientation correction is introduced. The determination of the orientation becomes possible with auxilliary software, exploring information form ORINP file. This far, only determination of the sensor axes deviations from nominal position is made using data from the magnetometer. The statistical examination of these results is also used to control the sensor location, that of the magnetic axes respectively, with regard to the physical axes of the object. Further options are foreseen to use the sensors for the angular velocities determination, as well as to provide solar sensor determination of the actual orientation. The orientation correction will be introduced solely for the cases when the processing data cannot be interpreted unifold. ORINP file can be used also for the determination of the orthogonality of the sensor axes. For the purpose, a Fourier series are used for the data of the differences between the theoretical and measured module of the field. This processing is also made after auxilliary software.

The software system is realized in operational medium DOS-ES, excluding the navigation programme, elaborated by Prohorenko into operational medium OS [5].

The requirements to the machine configuration are as follows: main memory 300 kb; disc drives — 2 pc 2314; magnetic tape drives — 3 pc; punched card input; line printer output.

The system exploration has shown it reliable and simple in performance.

Acknowledgements

The authors are grateful to Dr. I. Arshinkov for his help during the algorithmic developments of the problem and to Dr. P. Rendov for the valuable consultation during the organization of the software technological range.

References

1. Serafimov, K. B., I. S. Arshinkov, A. Z. Bochev, M. H. Petrunova, G. A. Stanev, S. K. Chapkunov. A measuring equipment for electric and magnetic fields in the range of the ionosphere-magnetosphere plasma, mounted aboard the INTERCOSMOS-BULGARIA-1300. — Acta Astr., 9, 1982, 397.
2. Langel, R. A., R. H. Estas. The near-earth magnetic field determined from MAGSAT data. — J. Geophys. Res., 90, 1985, 2495.
3. Bochev, A. Z. Coordinate transformations of magnetometer data from near-earth satellite. — Preprint No CLSR-85-01.
4. Bochev, A. Z., I. S. Arshinkov, A. P. Venedikov. Deviations of measured magnetic field with respect to the theoretical one as an orientation of magnetometer axes. — Compt. Rend. l'Acad. Bulg. Sci., 39, 1986.
5. Прохоренко, В. И. Описание универсальной программы рассчета навигационной информации о положении искусственного спутника Земли. — Препринт ИКИ АН СССР № 263, 1976, 80.

Программа ЭВМ о координатных трансформациях при замерах вектора магнитного поля

А. З. Бочев, С. Ц. Хаджистоянов, Н. Б. Истатков, Х. М. Георгиев

(Резюме)

Исследование продольных токов в ионосферно-магнитосферной области осуществляется на основе трансформации данных, полученных от непосредственных замеров вектора магнитного поля в геофизической координатной системе. С помощью этой программы обрабатываются данные трехкомпонентного магнитометра с автоматическим растяжением диапазона. В качестве входных данных используются географические координаты точек наблюдения и телеметрические данные компонентов, которые задаются в орбитальной координатной системе. Основные операции программы следующие: отбрасывание ложных кадров, преобразование телеметрических данных в физические величины; трансформация измеренного вектора в геофизическую координатную систему, включающую координаты относительно эксцентрического диполя; вычисление разностей между наблюдаемым и модельным полями.

При написании программы осуществлена оптимизация операций вход — выход. Большинство программ, написанных на PL—1, структурировано. Данные читаются большими порциями, что делает программу более удобной для пользования.

Bulgarian Academy of Sciences

Space Research in Bulgaria, 6

Sofia . 1990

A complex satellite experiment of investigating aerosolic optical properties in the atmosphere

Vera S. Petrova

Space Research Institute, Bulgarian Academy of Sciences, Sofia

Aerosols substantially affect the thermal regime of the Earth-atmosphere system by scattering and absorbing large portion of the sun irradiation in all spectral ranges. Therefore, the investigation of the optical properties of the aerosols in the earth atmosphere via satellite systems is of significant importance for the solution of many problems of climatology, meteorology, geospace research, environmental pollution, etc.

This paper considers the possibilities of a satellite radiational experiment providing for determination of the spectral and spatial dependence of the main optical characteristics of the aerosols: coefficient of scattering, indicatrix of scattering $\gamma_\lambda(h)$ and optical thickness $\tau_{a\lambda}(h) = \int_h^H \sigma_{a\lambda}(l)\, dl$.

Figure 1 illustrates the block-diagram for the measurements. Let us suppose that the observer is situated at a height H above the Earth surface. It

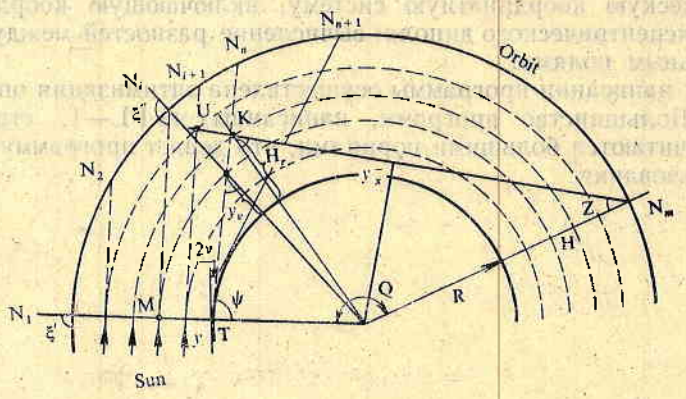

Fig. 1

is assumed that the atmosphere represents a sphere of radius $R_n > R$; (R — Earth radius) and is subdivided into n layers of radii $R_1, \ldots, R_n$ ($R_i = R + \Delta h_i$). We have incident parallel flux of solar irradiation at the outer atmospheric side. In the area of the terminator ($N_1 - N_n$) the experiment includes sequential measurements on the intensity of the scattered irradiation sunward and in nadir, and within the time interval $N_{n+1} = N_m$ when the space vehicle is in the earth shadow — scanning by horizon altitude was made. When the sun is spectrometered through the atmosphere, the intensity is determined by the unifold scattered and weakened by atmosphere irradiation $I_{1\lambda}$ and the intensity of the multifold scattered irradiation $I_{d\lambda}$:

$$(1) \qquad I_\lambda(s, y) = \frac{P_{u\lambda}}{M_y}\{I_{1\lambda}(s, y) + I_{d\lambda}(s, y)\},$$

where $P_{u\lambda}$ is a hatch transmission function (in observations from an orbiting station). $M(y)$ defines the weakening of the irradiation in the result of refraction divergence [1] at perigee height on the line of sight y, $I_{s\lambda}$ is the intensity of the solar irradiation outside the atmosphere for the spectral range of registration $\Delta\lambda$. Based on the transmission theory,

$$I_{1\lambda} = I_{s\lambda}\, e^{-2m_\xi \int_y^H \sigma_\lambda(l)\,dl} P_\lambda(y, s),$$

$$I_{d\lambda}(s, y) = \int_y^H e^{-(\tau_\lambda - \tau_{1\lambda})m_\xi} \cdot \sigma_\lambda \frac{(h)}{4\pi} \cdot \int_{4\pi} p_\lambda(s, s'; h)\, I'_\lambda(s, s'; h) P_\lambda(s, h) d\omega\, m_\xi\, dh,$$

where $\tau_\gamma = \int_y^H \sigma_\lambda(l)\,dl$, $\tau_{1\lambda} = \int_h^H \sigma_\lambda(l)\,dl$, $p_\lambda(s, s'; h)$ is a scattering function, $s(\xi, A)$ determines the direction of sight, ξ and A are zenith and azimuthal solar angles, $I'_\lambda(s, s'; h)$ is the intensity of a light flux, propagating at height h for direction s, $P_\lambda(s, y)$ is an absorption function of atmospheric gases into the investigated spectral range, $\sigma_\lambda(h)$ is a scatter cross-section, $\sigma_\lambda(h) = \sigma_{a\lambda}(h) + \sigma_{R\lambda}(h)$, $\sigma_{a\lambda}(h)$, $\sigma_{R\lambda}(h)$, are coefficients of aerosolic and Rayleigh scatter, m_ξ is an air mass. In a random point M of the terminator area, the solar irradiation intensity is determined with the expression:

$$(2) \qquad I'_\lambda(s, h) = I_{s\lambda}\, e^{-m_{\xi_T} \int_h^\infty \sigma_\lambda(l)dl} P_\lambda(\xi_T, h).$$

In an elementary volume dV, including point M, there occurs irradiation scatter in all directions, as well as towards the observer. Along the path from the scattering point to the observer, the intensity of the light flux varies in the result of the scatter processes due to molecules and aerosolic particles and to absorption from atmospheric gases into the MN layer. For the intensity in point N_n within the terminator area we obtain:

$$(3) \qquad I_\lambda(H) = \int_0^H I'_\lambda(h) e^{-\tau_\lambda(h)} P_\lambda(h) \sigma_\lambda(\xi_T, h) dh,$$

where $\sigma_\lambda(\xi_T, h)$ is a volumetric angular coefficient of scattering at height h.

At the moment N_i the intensity registered in nadir is determined by the intensity of the solar irradiation, weakened in the layer (y_v, H) as the lower atmospheric layers are not illuminated by the sun and do not contribute to the scattering of the direct solar irradiation. Similar to (3), we obtain for the intensity in point N_i:

$$I_\lambda(y_v)=\int_{y_v}^{H} I''_\lambda(h)e^{-\int_h^H \sigma_\lambda(l)dl} P_\lambda(h)\sigma_\lambda(\omega, h)\,dh, \tag{4}$$

where y_v is determined by the crossing point of the line of sight with a solar beam with perigee $y=0$ km, $y_v=\frac{R\sin\psi}{\sin\varepsilon}-R$, ω is the angle of scatter; $\psi=90-2\nu$, ν — angle of refraction.

$$I''_\lambda(\varepsilon, h)=\frac{I'_\lambda(h_1)}{M(h)}e^{-m_\varepsilon\tau_{5\lambda}(h)}P_\lambda(\varepsilon, h)+I_{d\lambda}(\varepsilon, y_v),\quad h_1=h-y_v,\quad \tau_\lambda=\int_{h_1}^{y_v}\sigma_\lambda(l)\,dl. \tag{5}$$

The light scattered into the atmosphere becomes the main source of light after sunset, when the atmosphere is illuminated by the beams of the sunset. In addition, the lower atmospheric layers situated in the earth shadow are not illuminated by the sun and are not incorporated into the scatter from the direct solar irradiation. During the scanning at the horizon height (N_{n+1}, N_m), the observer is to be found into the planet shadow and the line of sight is located at the altitude y_x above the Earth surface and in point K at altitude H_r enters the sun-illuminated area. Based on the theory of transmission, following the propagation and scatter of irradiation along the beam path up to a random point U and into the direction of the line of sight KN, we obtain for the registred intensity at scanning by the horizon height:

$$I^{\mathrm{IV}}_\lambda(s, y_x)=P_{u\lambda}I^{\mathrm{IV}}(s, y_x)e^{-m_z\tau_{6\lambda}}P_\lambda(s, h)+\int_{y_x}^{H} e^{-(\tau_{6\lambda}-\tau'_{6\lambda})m_z}\frac{\sigma_\lambda(h')}{4\pi}\cdot \int_{4\pi} p(s, s'; h')I'^{\mathrm{IV}}_\lambda(s, s'; h')\,d\omega\sec z\,dh', \tag{6}$$

where $\tau_{6\lambda}=\int_{y_x}^{H}\sigma_\lambda(l)dl$, $\tau'_{6\lambda}=\int_{h}^{H}\sigma_\lambda(l)\,dl$, $I_\lambda(s, h)$ is the intensity in the perigee of the line of sight y_x.

$$I^{\mathrm{IV}}_\lambda(s, y_x)=I^{\mathrm{III}}_\lambda(s, H_r)e^{-m_\gamma\tau_{5\lambda}}P_\lambda(s, y_x)+\int_{y_x}^{H_r} e^{-m_\gamma(\tau_{5\lambda}-\tau'_{5\lambda})}\frac{\sigma_\lambda(h)}{4\pi}\int_{4\pi} p(s, s', h)\cdot I'^{\mathrm{III}}_\lambda(s, s', h)\,d\omega\sec\gamma\,dh, \tag{7}$$

$\tau_{5\lambda}=\int_{y_x}^{H_r}\sigma_\lambda(l)\,dl$, $\tau'_{5\lambda}=\int_{h}^{H_r}\sigma_\lambda(l)\,dl$, $I^{\mathrm{III}}_\lambda(s, H_r)$ is the intensity in point K, determined as a sum of all the elements into direction KN.

(8) $$I_\lambda^{III}(s, H_r) = \int_{H_r}^{\infty} I_\lambda^{VI}(s, h) e^{-m_\gamma \tau_{3\lambda}} p_\lambda(\gamma, h)\, \sigma_\lambda(\eta, h)\, dh,$$

$$\tau_{3\lambda} = \int_{H_r}^{h} \sigma(l)\, dt,\ I_\lambda^{VI}(s, h)$$ — irradiation intensity at random point U.

(9) $$I_\lambda^{VI}(s, h) = \frac{I_{\lambda s}}{M(h)} e^{-m\xi'' \tau_{2\lambda}} P_\lambda(\xi'', y) + \int_y^h e^{-\sec\xi''(\tau_{2\lambda} - \tau'_{2\lambda})} \frac{\sigma_\lambda(h')}{M(h')\, 4\pi} \int_{4\pi} p(s, s'; h') \cdot I'_\lambda(s, s', h')\, d\omega \sec\xi''\, dh',$$

$$\tau_{2\lambda} = \int_y^h \sigma_\lambda(l)\, dl,\ \tau'_{2\lambda} = \int_y^{h'} \sigma_\lambda(l)\, dl,$$ η — angle of scatter, $\cos\eta = \cos\varepsilon \cdot \cos\gamma + \sin\varepsilon \cdot \sin\gamma \cos A$.

Equations (1), (3), (4), (6) are basic equations of transmission into the complex radiational experiment including spectrometry of direct solar irradiation, nadire measurements into the terminator area and scanning of the horizon. They represent sophisticated functional dependences of the measured intensities of the scattered solar irradiation due to the atmosphere optical properties, namely to layers where it propagates. Initially, the spectral, vertical and spatial dependence of $\sigma_{a\lambda}(h)$ is determined in unifold scatter approximation. It is assumed that in each sublayer of the atmosphere the aerosolic scatter coefficient is presented by exponential approximation $\sigma_{a\lambda}(y_i) = \sigma_{a\lambda}(y_{i-1})\, e^{-\beta h}$, which is effective at high resolution of the experiment by altitude. We obtain for the optical thickness in the i th sublayer:

(10) $$\Delta\tau_{a\lambda}(y_i) = \frac{\sigma_a(y_{i-1})\,(e^{-\beta_i y_{i-1}} - e^{-\beta_i y_i})}{\beta_i}.$$

But for the case of single scattering with regard to the registred direct solar irradiation in two subsequent moments N_i and N_{i-1}, we obtain for $\Delta\tau_a(y_i)$:

(11) $$\Delta\tau_{ai} = \frac{1}{2m_\xi} \ln \frac{I_\lambda(s_i, y_i) M(y_i) P_\lambda(y_{i-1})}{I_\lambda(s_i, y_{i-1}) M(y_{i-1}) P_\lambda(y_i)} - \int_{y_{i-1}}^{y_i} \sigma_{R\lambda}(y_{i-1}) e^{-ah}\, dh.$$

Hence, for the aerosolic scatter coefficient in i layer we define:

(12) $$\sigma_{a\lambda}(y_{i-1}) = \frac{\Delta\tau_{a\lambda_i} \beta_i}{e^{-\beta_i y_{i-1}} - e^{-\beta_i y_i}}.$$

The relationship between $\sigma_{a\lambda}(y_{i-1})$ and $\sigma_{a\lambda}(y_{i-2})$ is given with:

(13) $$\sigma_{a\lambda}(y_{i-1}) = \sigma_{a\lambda}(y_{i-2})\, e^{-\beta_{i-1} y_{i-1}}.$$

For the last layer (where we may assume lack of powerful aerosolic layers) $\beta_n = 1/H_0$, H_0 is the height of the isothermal atmosphere. For the other layers β_i is determined by (1). The method provides for high-accuracy definition of $\sigma_{a\lambda}(h)$ into the upper atmospheric layers, where the contribution of

the multifold scatter is insignificant also for spectral range, distinguished by lack of absorption from molecules of gas with variable density (O_3, H_2O). The altitudinal adjustment of the spectrometric record when scanning the horizon is made by comparing the ratio between the atmospheric transmission

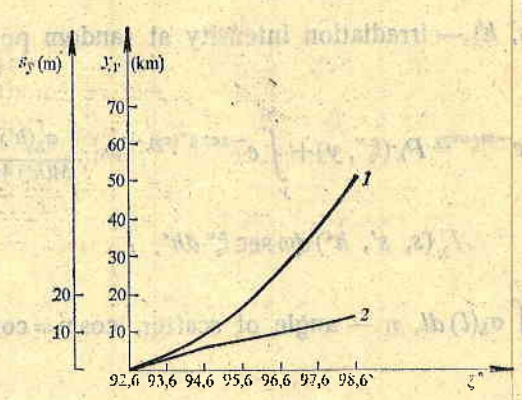

Fig. 2. Variation at the height of sight and the resolution in altitude in dependence on the fast performance, equipment sensibility and solar zenith angle. *1* — y_v; *2* — s_y

function in the i th layer and that at $y_x = y_{min}$ in the spectral range 0.76 μm and the ratio of the registred intensities within the same spectral range [2]. The method allows for precise altitudinal adjustment, since the transmission function of the oxygen is computed with high accuracy. It is necessary to make complex measurements in the optical and near IR ranges, as well as of the natural irradiation in the radio range for the spectral ranges specified with water vapour absorption. This allows to determine the integral water content required for the computations of the transmission function in the studied atmospheric layer.

The altitudinal resolution at nadir measurements in the terminator area depends on the fast performance and the sensitivity of the measuring equipment. Figure 2 shows the variation at the height of sight y_x and the resolution in altitude $s_{y_i} = y_{v_i} - y_{v_{i-1}}$ in dependence on the fast performance, the measurement equipment sensitivity and the zenith angle ξ of the sun. From the ratio of the registered intensity in two sequential moments for the optical thickness in the layer y_{v_i}, $y_{v_{i+1}}$ we obtain:

$$\Delta\tau_{a\lambda_i} = \frac{1}{m_\xi - 1} \ln \frac{I_{i\lambda} \int_{y_i}^{y_{i+1}} P_\lambda(\varepsilon, l)\, dl}{I_{i+1,\lambda} \int_{y_i}^{y_{i+1}} P_\lambda(l)\, dl} - \int_{y_i}^{y_{i+1}} \sigma_{R_\lambda}(l)\, dl. \tag{14}$$

The coefficient of the aerosolic scattering $\sigma_{a\lambda}(h)$ and β_i are computed on the basis of dependencies similar to (10)-(13).

The values obtained for the spatial and vertical dependencies of $\sigma^0_{a\lambda}(h)$ are used as input values for the solution of the transmission equations (1), (3), (4), (6) by the Monte Carlo simulating modelling method. The determined

values of the spectral and vertical dependencies of $\sigma_{a\lambda}(h)$ are obtained by minimization of the functional:

$$\sum_{i=1}^{m} (\tilde{I}_{i\lambda} - I^k_{i\lambda}(\sigma^k_{a\lambda}(h)))^2 = \delta, \tag{15}$$

where $\tilde{I}_{i\lambda}$ is the measured value in point $i(s_i, y_i)$, $I^k_{i\lambda}$ the value obtained for the intensity in the numerical modelling of the respective equation of transmission after the Monte Carlo method, where $\sigma^k_{a\lambda}(h)$ varies according a determined law, $\sigma^k_{a\lambda}(h) = \sigma^{k-1}_{a\lambda}(h) - f(\delta)$, k — number of iteration.

The proposed radiation experiment is partially realized aboard the SALYUT-6 [4] orbiting station, while the complex version between visible, near IR and radio ranges was made aboard METEOR-PRIRODA within the BULGARIA-1300-II project [3].

References

1. Розенберг, Г. В. Сумерки. М., 1963.
2. Петрова, В. С. Изследване на стратификацията на аерозолната компонента в атмосферата чрез спектрометриране на хоризонта с многоканалната система „Спектър 15" от орбиталния комплекс „Салют 6". II. Млад. сесия 1983.
3. Mishev, D., V. Petrova, G. Ivanov, A. Krumov, T. Nasarsky. Complex study of the atmospheric and ocean state by data from the scientific equipment installed on "Meteor Priroda" satellite. 7-13 Oct. 1984. Suitz. IAF.
4. Мишев, Д., В. Петрова, С. Ковачев, П. Петров, В. Рюмин, А. Симонов. Дистанционные исследования параметров атмосферы по спектрометрическим измерениям аппаратуры „Спектр — 15" со станции „Салют — 6". Межд. симп. Исслед. прир. рес. Земли с орб. станции „Салют — 6" 21-2: II. 1983. Душанбе, СССР.

Комплексный спутниковый эксперимент по исследованию оптических свойств аэрозоля в атмосфере

В. Д. Петрова

(Резюме)

Рассмотрены возможности спутникового радиационного эксперимента, позволяющего определить спектральный и пространственный ход основных оптических характеристик аэрозоля: коэффициент рассеяния, индикатриса рассеяния и оптическая толщина.

Предложенный эксперимент частично реализован на станции „Салют — 6", причем комплексирование видимого, ближнего ИК и радиодиапазона сделано на ИСЗ „Метеор — Природа" по проекту „Болгария — 1300".

Bulgarian Academy of Sciences

Space Research in Bulgaria, 6

Sofia . 1990

Data acquisition system for complex and synchronous geonomic and space investigations

Dimiter N. Mishev, Angel M. Angelov, Garo H. Mardirosyan, Boiko. H. Tsenov, Mihail F. Fratev, Atanas K. Madjirov**

Space Research Institute, Bulgarian Academy of Sciences, Sofia 1113
**V. I. Lenin Higher Mechanical and Electrical Engineering Institute, Sofia*

The problems, methods and technical means for remote sensing of the Earth represent a sophisticated multinode system, where suborbital (and mainly ground-based) systems and complexes for data acquisition and processing occupy a major place. Data and information obtained from ground-based measurements not only complement and make possible the efficient data processing of information obtained by satellites, manned space vehicles and orbiting research laboratories. Simultaneously, they represent exclusively valuable material necessary for the solution of completely independent scientific fundamental and applied problems, as well as economic tasks in the field of geophysics, geology, geography, meteorology, hydrology, natural resource studies, ecology, agriculture, etc. Due to the broad scale of these studies and the large territories over which they must be implemented, as well as to the requirements for their synchronous realization for the majority of cases, it is useful and even imperative to apply radiotelemetric systems for data acquisition.

Within the framework of the BULGARIA-1300 space project [1], a data acquisition system for complex and synchronous geonomic and space investigations — DAS was developed at the Central Laboratory for Space Research of the Bulgarian Academy of Sciences. This system is the main device within the equipment facility of the Universal Mobile Laboratory for Conplex Geonomic Investigations (UMLCGI) and the Mobile Ground Station for Synchronous Satellite Investigations (MGSSSI) [2].

The data acquisition system — DAS is developed for automatic telemetric acquisition (transmission, receiving and registration) of digital information at synchronous and complex geonomic and space investigations. Generally, this information includes data on: spectral reflectance and natural emissivity of natural objects; temperature of the surface soil and contact air layers; humidity and electroconductivity of the surface soil layer; earth magnetic field parameters; atmospheric pressure; wind direction and velo-

city in the contact atmospheric layers; wave motion, current direction and velocity of rivers and other water basins; aerosolic particle density into the atmosphere; microseismic background and seismic fluctuations, etc.

The most general principle of DAS performance is based on the automatic switching of the respective peripheral points at determined time-intervals

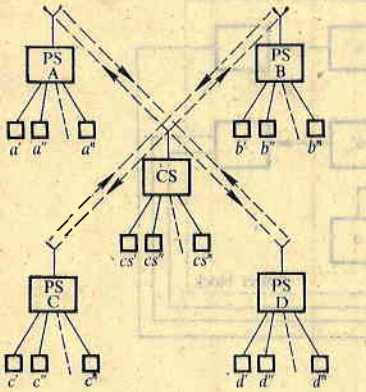

Fig. 1

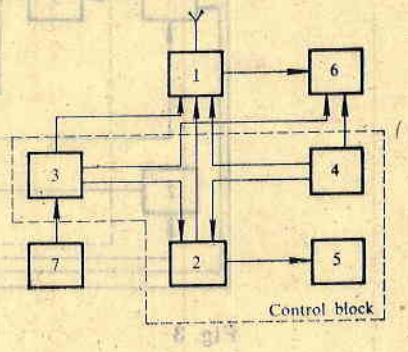

Fig. 2.

and information transmission for receiving and registration into a central point. The telemetric switching of the individual peripheral points is made via radiosignal emissions from the central point, modulated by different tone frequencies. The performance management of the entire system is made in the following manner: a) by hand, b) by instrumental program device, c) by microprocessor control.

Initially, it was reasonable to develop a DAS system incorporating one central and four peripheral points — DAS-5, i. e. with a possibility for information acquisition from 5 points.

The central point (CP) is mounted as in UMLCGI and MGSSSI or as in a stationary observatory. From there, the operation of the peripheral points (PP) is controlled and the receiving, registration, visualization, as well as primary and partial data processing are effected. Figure 1 illustrates the symmetric situation of the peripheral points PP-A, PP-B, PP-C, PP-D with regard to the central point CP of DAS-5. In dependence on the research goals and the conditions for their implementation this situation may vary widely. The different measurement instruments and sensors are connected with the central and peripheral points via cable links and may be located in various configurations at distances to several tens of the meter.

The receiving-transmitting DAS part is realized on the basis of USW radiostations.

Figure 2 shows the principal block-diagram of the CP in a program device controlled version. The operation of the radiostations *1* and the registration block *6* are controlled by a control block, the main subblocks of which are: *2* — tone generator block containing 5 tone generators; *3* — program block, *4* — hand operated block, *5* — indication. The program block *3* represents a device of the Universal Program Device for Geophysical Observatories (UPDGO) type [3] is joined to an electronic clock *7* with quarz generator for synchronization, with a possibility for automatic verification by reference radiosignals for exact time, for example the Exact Time System (ETS) [4].

The main node of the peripheral points (Fig. 3) is the selective block containing: amplitude reducer — *3;* active narrow band filters, the first *(4)* being adjusted to the respective tone frequency f_A, f_B, f_C or f_D, and the second *(5)* at the starting frequency f_{st}; keys — *6;* time releys — *7;* comparator — *8* and

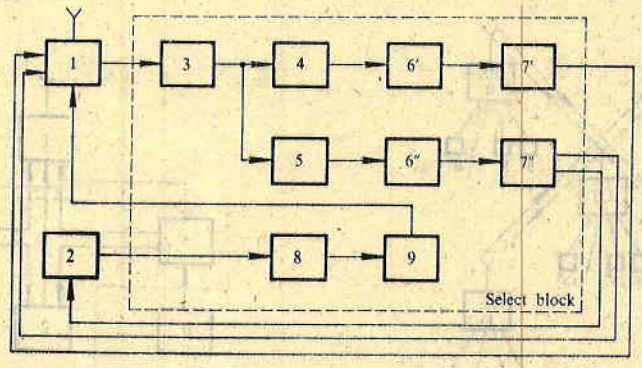

Fig. 3

forming device — *9*. The signals received by radiostation *1* are supplied to the selective block, which operates the radiostation and the data source, when she frequency corresponding to the peripheral points is received: the radiostation is reswitched from "service receive" mode into "transmission" mode and the data source *2* is switched to the radiostation input. The data source includes a coding device and different meters, transforming the investigated parameters into electric signals. These electric signals are supplied via multiplexor to an analog-to-digital converter from where a 10-bits signal is obtained. One bit is added to this signal for "start" and one for "stop." A third bit is also added for verification by evenness.

Service telephone calls are also made with the radiostation in addition to the data receiving and transmission.

The data transmission rate for DAS-5 is 1200 bit/sec. The selected radiostations provide the required reliability under this relatively low rate. One of the conditions for the normal functioning of the DAS system is the optimum situation of the peripheral points with consideration of all effects in such USW connection.

The radiostation of the peripheral point operates routinely into "service receive" mode. The sensors and instruments measuring the respective parameters within the block of data source are switched and transmit information only by call from the respective peripheral point. Hence, the high-level requirements to the performance of the selective block which is located between the radiostation and the data source. It can be seen from the mentioned above that mainly parameters of relatively slow variation are measured but many digital data are taken. The continuous observation of the peripheral station would result into large surplus in the registration. The periodical taking of information may be accompanied with errors from radiochannel gaps to the respective point or measurement device. Then, with the rigid instrumental program device realization, a data repetition should be requested, i. e. there is a danger of violating the registration cycle.

The microprocessor control of the DAS system provides for the implementation of the following control modes for the central and the peripheral points:

1. Cyclic switch of all peripheral points, taking of data from all the measuring devices and logical processing of the results. If the latter do not corre-

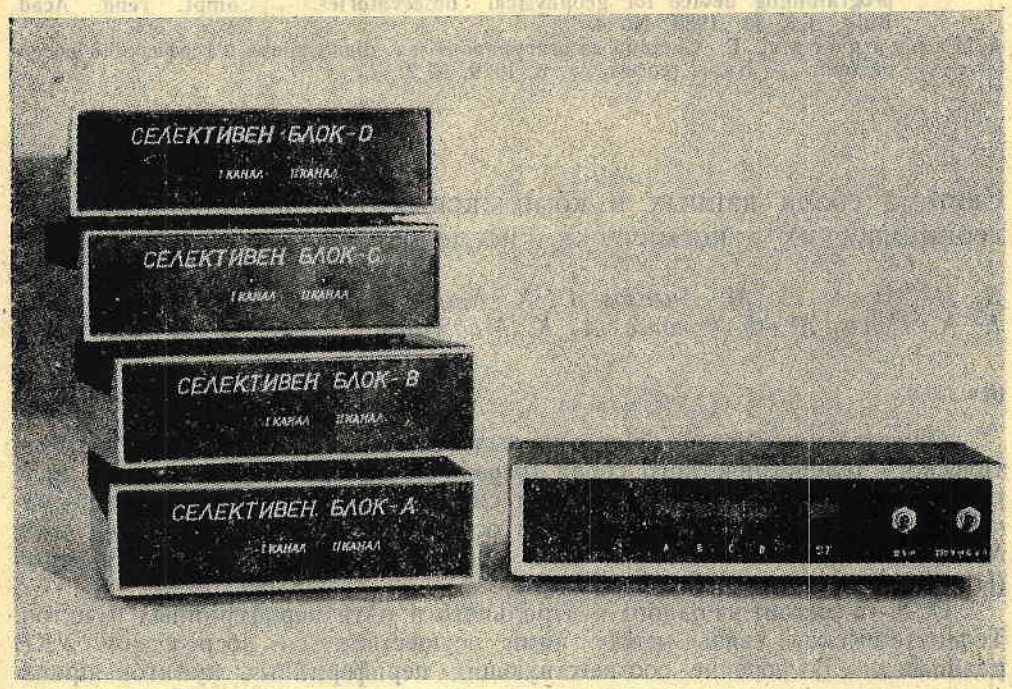

Fig. 4. A general view of the peripheral points and of the central point

late with the previous ones, the error, its occurence and location may be identified.

2. Priority switching of measuring devices with large dynamics into the registration process or with frequently occuring errors, and control of one or several parameters. The registration is made only if the results are considered adequate.

3. Cyclic switch-in of all the points and taking of data on the most rapidly varying parameters only.

4. Digital filtering and elimination of errors by averaging the results.

The system does not restrict the number of included points and measuring devices, if they guarantee the provision of normal measurement. Naturally, on the basis of the described system for data acquisition for complex and synchronous geonomic and space investigations it is possible to develop a more specialized version, for example for synchronous satellite studies, for magnetic investigations, for seismological research, for the needs of hydrology, etc., which is simpler and of a greater operational capacity.

References

1. Научна програма „БЪЛГАРИЯ-1300-II", ЦЛКИ-БАН, София, 1980.
2. Мишев, Д., Г. Мардиросян, Д. Инджева. Подвижна наземна станция за синхронни спътникови измервания. — Списание на БАН, 17, 1982, № 3.
3. Mishev, D. N., G. H. Mardirosyan, S. K. Jivkov. Universal programming device for geophysical observatories. — Compt. rend. Acad. Bulg. Sci, 33, 1980, No 4.
4. Мардиросян, Г. Система за осигуряване на точно време в геофизични обсерватории. — Бълг. геофиз. сп. 5, 1979, № 2.

Система сбора данных в комплексных и синхронных геономических и космических исследованиях

Д. Н. Мишев, А. М. Ангелов, Г. Х. Мардиросян, Б. Х. Ценов, М. Ф. Фратев, А. К. Маджиров

(Резюме)

Описываемая система сбора данных (ССД) предназначена для автоматического телеметрического сбора (передачи, приема и регистрации) цифровой информации в комплексных и синхронных геономических и космических исследованиях. Она является основным узлом аппаратурной части Мобильной наземной станции для синхронных спутниковых измерений (ПНСССИ).

ССД—5 состоит из одного центрального и пяти периферийных пунктов. Телеметрическая связь между ними осуществляется посредством УКВ радиосвязи. Включение соответствующих периферийных пунктов производится автоматически по команде с центрального пункта. Микропроцессорное управление ССД обеспечивает достижение высокой оперативности, осуществление различных режимов работы, а также первичную обработку данных на самом месте проведения исследований.

Коротко описаны основные блоки ССД, даны некоторые технико-эксплуатационные характеристики, рассмотрены различные типы организации работы.

Bulgarian Academy of Sciences

Space Research in Bulgaria, 6

Sofia . 1990

Interference light filter shifting device for the EMO-5 satellite photometric system

Nencho P. Petkov

Space Research Institute, Bulgarian Academy of Sciences, Sofia

In satellite photometric equipment for studies of weak optical emissions interference light filters and common photoconverter and measurement track are used to separate the spectral lines measured by illumination intensity [1, 2, 3, 4]. This combination substantially decreases size, weight and power consumption, but requires mechanical shifting of the different light filters in front of the photoconverter. To meet the requirements of a specified law of motion of the light filters, a discrete drive by step drivers is most frequently used.

Two kinematic chains with discrete drive are used in the EMO-5 photometric system, working as part of the complex of scientific equipment aboard the INTERCOSMOS-BULGARIA-1300 satellite. They provide for measurement the illumination intensity in 6 spectral lines, periodical calibration at flight time, and obtaining of images of illuminated areas in one spectral line. We shall consider here the specifics and shall describe the principle of control of the interference light filter shifting in the EMO-5 photometric system.

The block diagram of the device for shifting the interference light filters in the EMO-5 system is shown in Fig. 1. The following conditions have been observed in this design: provision of 8 measurement positions (6 spectral lines, reference source for calibration and position for drift measurement of the photoconverter); exact setting of each cyclically repeated position in front of the photoconverter for a specified time period; reliable operation of the mobile parts in vacuum and within the temperature range of -20 to +50° C, small size, low weight and power consumption; objective control over the measured positions.

The six interference light filters, the reference source and the position for drift measurements are situated evenly along a rotating disc (F VV). The rotation of FVV is effected by a discrete drive with a step driver and is synchronized by 1 s pulses (SP) from the board system for universal time. In order to provide the exact determination of each position of FVV, the step driver

with a reductor (SMR) is controlled by the position of the driven shaft via position keys (PS) of optoelectron type. Pulses are produced for each measurement position (FP) and for the beginning of each new cycle (CD) of the FVV rotation, with respective duration of τ_{FP} and τ_D.

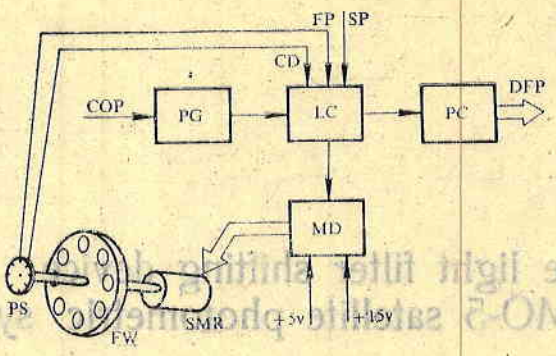

Fig. 1

The necessary time period Δt_M for the measurement of each position is determined by the requirements of the photoconverter. For a time Δt_M, FVV should be reliably fixed in one of the eight measurement positions, and then shifted to the next one. Due to the motion of FVV in one direction, the control block (MD) of SMR is of the irreversible type. The block for logical control of the motion (LC) provides the time period Δt_M, as well as the period Δt_D, allowing the FVV motion in dependence on the PS state. The step driver makes N steps in order to shift FVV at an angle θ_{FP} to the next position:

$$N = \frac{\theta_{FP}}{\pi K_j} P, \tag{1}$$

where K_j is the coefficient of reduction; P — parameter of the step driver, depending on the type and commutation of its wiring.

The precision of fixing FVV in a given position is $\theta_{FP} < K_j \frac{\pi}{p}$. An additional signal is introduced into the system so as to forbid the FVV motion from the comparator for optical protection (COP) of the entire photometric track of the EMO-5 system. When no signal is supplied by COP, the pulses from the output of a pulse generator (PG) enter LC. The information (DFP) on the position of FVV enters the telemetric system as a 4-order parallel code from the output of a counter for interference light filter positions (PC).

The logics of motion control may be illustrated with Fig. 2. The synchropulses SP with period T_{SP} are supplied to a frequency divider (FD) and a drive timer (T_1). Along with this they set up the monovibrator T_3 into starting position allowing the pulses from PG to enter via coincidence circuit (G_2) to MD so as to drive the step driver (SM). After T_1 the period is divided into time periods Δt_M and Δt_D, while Δt_D is computed with supplementary value with regard to the time necessary for the FVV motion between two adjacent positions. When FVV reaches a given position via the coincidence circuit (G_1), a pulse of duration τ_{FP} enters T_3 and drives it out of the starting position. A time period Δt_P is produced to forbid motion, where $\Delta t_P \geq \Delta t_M$. Simultaneously, a pulse of duration τ_{FP} enters PC to indicate the given position of FVV,

and the annuling of PC is effected by a CD pulse for the beginning of the rotation cycle. The sequential synchropulse with a period $2T_{SP}=\Delta t_M+\Delta t_D$ returns T_3 to starting position. (T_2) monovibrator is incorporated also in LC, producing a pulse of duration 100 ns.

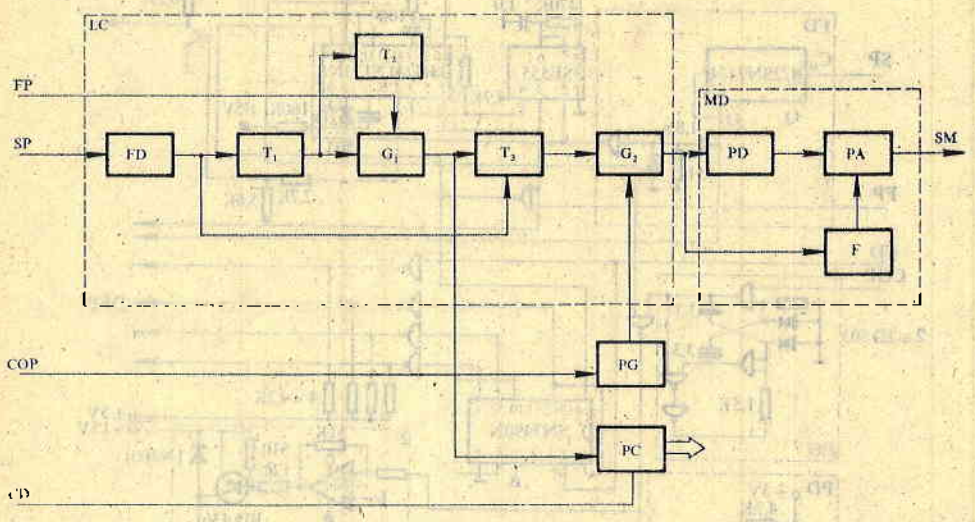

Fig. 2

The control block (MD) of the driver contains pulse distributor (PD), power amplifier (PA) and control circuit (F) for the current via SM wirings. PD transforms a unitary code into a m-phase system of rectangular pulses, where m is the number of wire commutation cycles, and F provides low consumption for time Δt_M.

The block electrical circuit of motion control of the interference filters into the photometric EMO-5 system is shown in Fig. 3. At $T_{SP}=1$ s, T_1 (SE555) provides time periods $\Delta t_D=0{,}5$ s and $\Delta t_M=1{,}5$ s with 2% precision. The monovibrators T_2 and T_3 are implemented on integral circuits SN54LS123N. No firm requirements with regard to the pulse generator (SN5400N) exist. The generator operates on frequency of 100 Hz. The pulse distributor (SN5474N) is of the irreversible type and transforms a unitary code into a 4-phase system of rectangular pulses. The power amplifier is unipolar, irreversible with transistor-diode keys (4×KFY18, 8×2D510A, 2×SN75450). The current through the step driver wiring is regulated via transistor (BD 436), controlled by an inverting amplifier.

A step driver of the CDA-15 type with two phases, active rotor and a single step of 15° is used into the motion device for the interference light filters. In order to safeguard its performance in space vacuum its bearings are replaced by the vacuum type TU370060 58-73, while the carriers of the different wires are produced from caprolon plastic. The reductor has a coefficient of reduction $k=1:10$, the driving wheel is made of steel brand 45. The driven wheel made of caprolon carries the light filters. The overall weight of the device is 290 g and the power consumption<2 Wt.

The device for shifting the interference light filters has successfully passed all the tests and operated within the EMO-5 photometric system aboard the

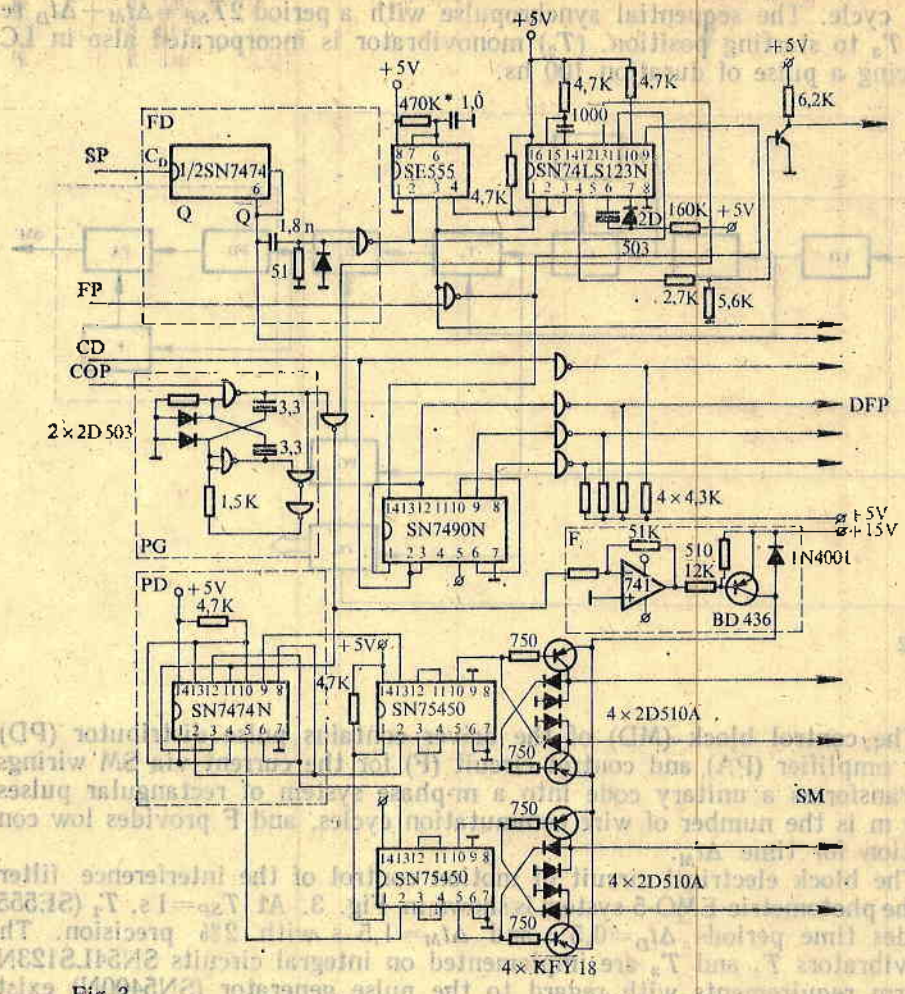

Fig 3

INTERCOSMOS-BULGARIA-1300 satellite. For one year, more than 300 hours of active operation can be reported for the EMO-5 system.

References

1. Reed, E. L., W. B. Flower, J. E. Blamont. J. Geophys. Res., 78, 1973, 5658.
2. M. Gogoshev, N. Petkov. Equipment of Outer Ionospheric Investigations. AN USSR, IZMIRAN, M., 1980, 186-195.
3. N. P. Petkov, M. M. Gogoshev, St. I. Sargoichev. Compt. Rend. Acad. Bulg. Sci. (in print).
4. Rank, L. A., J. D. Graven, K. L. Aceerson, M. R. English, R. H. Eather, R. L. Carovillano. Space Sci. Instr., 5, 1981, 369. 393.

Устройство для перемещения интерференционных светофильтров в спутниковой фотометрической системе ЭМО—5

Н. П. Петков

(Р е з ю м е)

Рассмотрены характерные особенности интерференционных светофильтров и описан принцип управления их перемещением в фотометрической системе ЭМО—5, участвующей в комплексе научной аппаратуры спутника Интеркосмос — Болгария — 1300. Даны блок-схема и короткие описания технико-эксплуатационных характеристик основных блоков. Показана и прокомментирована логика управления движения.

Bulgarian Academy of Sciences

Space Research in Bulgaia, 6

Sofia . 1990

Systems for laboratory testing of two-dimensional coordinate-sensitive detectors for charged particles

Peter T. Baynov, Yordanka V. Semkova

Space Research Institute, Bulgarian Academy of Sciences, Sofia

Introduction

Ground-based testing is the primary and important step towards the development of space research instruments. Some specific aspects of the testing are: capacity verification and element characteristics investigation of the detecting devices; — coordination between sensor and electronic block performance, calibration and tuning; development of control-and-measuring equipment; reliability testing, etc.

In order to perform this testing, we need systems of sufficient complexity and methodics, quite often with capacity and requirements exceeding those of the on-board systems. Thus, we provide the possibility of an adequate research of the circuitry potential and its optimisation. In order to obtain and investigate the correlative links and dependencies between the physical model and the experimental results, as well as to find out the virtual criteria of estimating the tests and the extent to which they approximate the actual conditions, we use relatively complicated and powerful soft- and hardware facilities.

The problem

A general purpose testing facility for charged particle detectors is shown in Fig. 1. The tested detecting element is placed into a vacuum chamber together with the charged particle source. The required conditions are transmitted via microcomputer to the controlling block which, in turn, supplies the detector operational parameters and the impact source.

The information obtained from the detector is addressed to the electronic block, where it is subjected to primary processing and read by the

microcomputer. Simultaneously, the information from the vacuum chamber and the electronic block is supplied to the control-and-measuring instruments: analog-to-digital analysers, oscilloscopes, etc.

Recently, many laboratory and space research investigations, related to charged particle registration use coordinate-sensitive detectors CSD, since

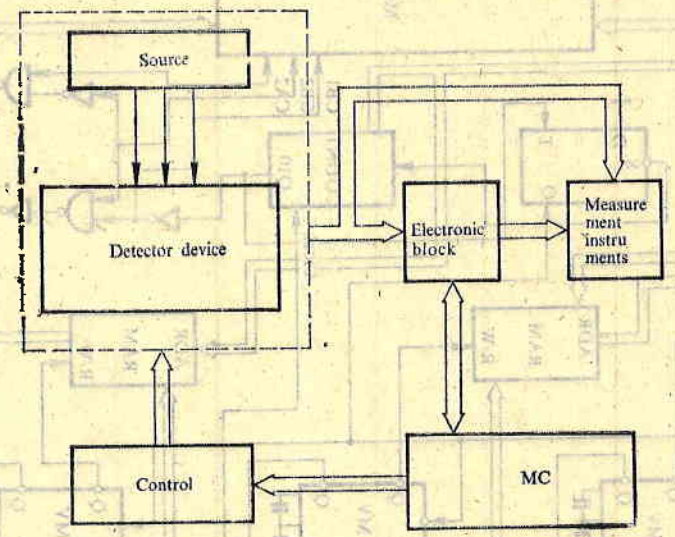

Fig. 1

they provide relatively easy and fast pattern of obtaining information on the particle location. The coordinate-sensitive detectors contain an input charge multiplying element (cascade-connected microchannel plates), and a trapped particle coding anode. Some CSD [1] are known to provide analog coding of the particle locations. There, the anode device divides the output charge from the microchannel plates between the terminals of the individual electrodes with relative amplitudes, depending on the particle location on the CSD. The distribution centroid of this charge and the trapped particle location is measured by the method of analog ratio. Three-electrode anodes are used in the CSD devices, as suggested in [1], for the determination of the trapped particle coordinates, i. e. it is necessary to measure the signals form these electrodes.

The electronic circuit

The block diagram of the electronic system, required for the laboratory testing of coordinate-sensitive detectors (CSD) of the type mentioned above, is shown in Fig. 2. The system is developed as a three-channel version in order to measure the respective CSD outputs.

The amplitude analysis circuit (AAC) is the unit connected directly with the particle detector, which defines the accuracy and velocity of registration and the consequent identification, processing and control procedures. On the other hand, it should ensure all the necessary conditions of adjusting an asyn-

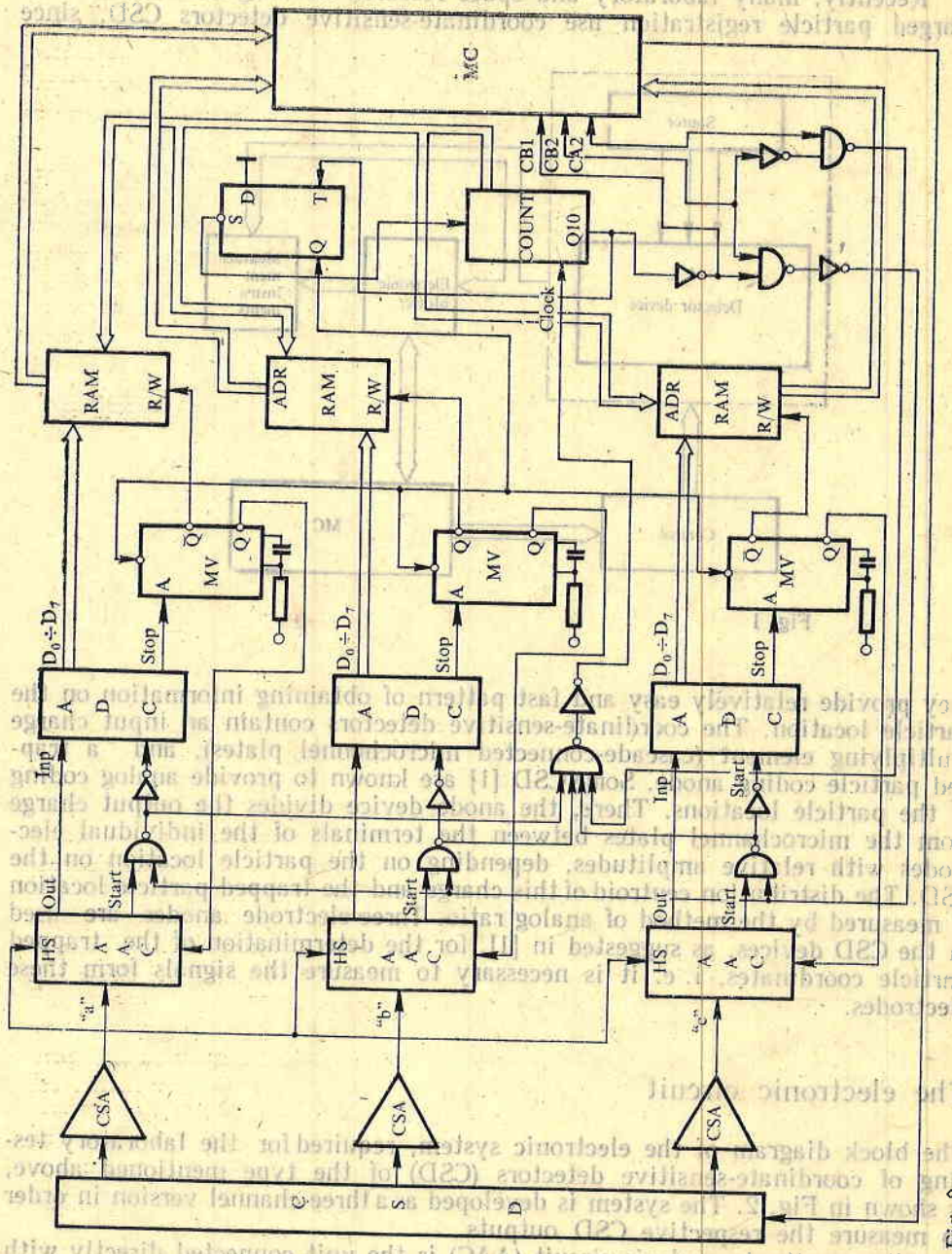
MC
CB1
CB2
CA2
COUNT
Q10
Clock
RAM
R/W
ADR
MV
Stop
Inp
Start
Out
HS
CSA
"a"
"b"
"c"
$D_0 \div D_7$

Fig. 2

chronous system to a synchronous, fast-performance system for processing and control. The amplitude analysis circuit determines to a great extent the adequate transformation of the particle spectrum into a signal spectrum, i. e. there is a possibility for the reverse process: reconstruction of the initial spectrum with sufficient accuracy. The analog signal shape of the detecting system and the specific requirements quite often determine a mixed type of structural-informative organization of the amplitude analysis systems under maximum requirements for real time performance.

The development and the operational capacity of the amplitude analyser is based on the technical capacity and characteristics of the detector. The two cascade-connected microchannel plates, which are the main element of the position-sensitive detectors, have amplification of 10^6-10^7 electrons per event and are specified with large spatial resolution, fast performance and low background signal. These major characteristics, together with the characteristics of the charge-sensitive amplifiers connected to the anode, define the cycle and the dynamics of the amplitude analysis, the main characteristics of which are:

— high resolution including processing of pulses of a width larger than 200 ns;

— fast performance, defined exclusively by the transformation time in the analog-to-digital converter ADC. For ADC of parallel conversion of time 100 ns (for 256 discretion levels), the time for the amplitude analysis is 400-500 ns per pulse, implementing TTL digital IC of 54. . . . . series;

— high precision and reliability of measurement, defined by the principle of net pulse measurement (guaranteed measurement from "zero" level of the input signal), by the lack of frequency correcting and tuning circuits etc.

The main operational modes in testing CSD are set up by the microcomputer MC, and measurement, analysis and processing are time-separated operations. This is required by the necessity of a detailed investigation of the CSD's capacity and characteristics under the effect of a controllable physical system, where much time and profound analysis are requested. The measurement cycle starts with the definition of the CSD parameters and the setting-up of the system into initial state. The pulses from the outputs of the respective CSA are fed to the inputs of the respective amplitude analysers AA. AA, in turn, memorize the maximum amplitude pulse values and shape signals for driving ADC. The first "start" signal enhances the counter (COUNT) content by a unit. The counter content determines the sequential cells of the RAM memories for the two channels, which registrate the digital code of the maximum amplitude value of each pulse. The measurement cycle is rejected when the memory is filled by the counter signal and the microcomputer shifts to a processing mode. For the purpose, it transfers the content from the two memories of the testing system into its own operational memory. The processing of these data is based on criteria and algorithms defined by the physical set-up of the measurements. Such a processing, for example, is the yield of the ratio $2a$, $(a+b+c)$ and $\frac{2b}{a+b+c}$ from the maximum amplitude values of the pulses from the three CSD outputs, obtained for the same time interval. The program realization comprises two parts. The first represents an assembling programme and refers to the experiment control, while the second relates to the computation of the upper ratios, the visualization and the graph display of the results, and to the amplitude and time distribution of the registrated signals, i. e. it is obviously developed on a higher level.

The entire system is specified with large dynamics and flexibility. It is both hard- and software opened and assumes expansion of instrumental and program functions and potential. The use of personal computer provides a possibility for long-term reliable testing and complex investigation of similar instruments and systems.

References

1. Martin, C., P. Jelinsky, M. Lampton, N. O. Anger. — Rev. Sci. Instr., 52, 1981, 1067.

Система лабораторных испытаний двухмерных координатно-чувствительных детекторов заряженных частиц

П. Т. Байнов, Й. В. Семкова

(Резюме)

Описана система для лабораторных испытаний и калибровки двухмерных координатно-чувствительных детекторов заряженных частиц. Детектор состоит из микроканальных пластин, связанных шевронно, и анода, осуществляющего аналоговое кодирование местопопадания частиц. Характеристики детектора измеряются в вакуумной камере при помощи электронного пучка. Электронная система определяет центроиду распределения заряда на детекторе, визуализирует полученные данные и управляет процессом измерения. Система включает персональный компьютер.

Bulgarian Academy of Sciences
Space Research in Bulgaria, 6
Sofia . 1990

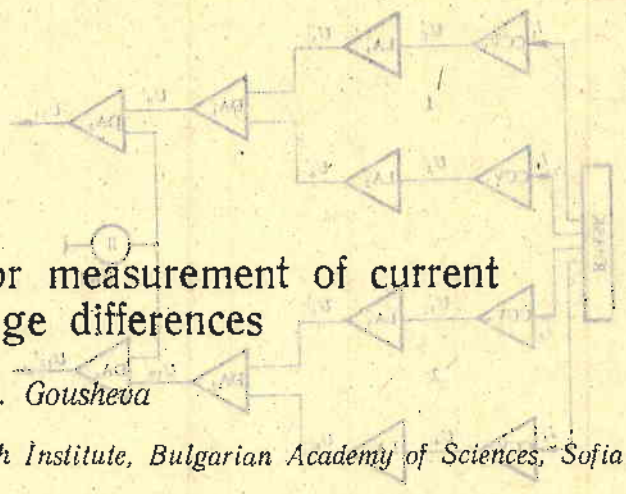

Device for measurement of current and voltage differences

Mariana N. Gousheva

Space Research Institute, Bulgarian Academy of Sciences, Sofia

Besides measurements of absolute values of physical parameters, other problems related to the determination of relatively dimensionless values also exist. In them, the ratio between two electric values is a measure determining the measured value.

Such a problem occurs in the measurement of the perpendicular component of the ion drift velocity in the ionosphere, where a multigrid flat trap with separated four-section collector RPASC is used as a preliminary transformer of the non-electric value into an electric one and, hence, we look for the ratio between currents $\frac{I_1}{I_2}$ and $\frac{I_3}{I_4}$ from the four sections of the collector. The ion arrival angle on the four sections of the collector is determined via measurement of the differential difference of currents from two couples of opposite sections, for which it is necessary to orient the perpendicular trap axis along the container vector [1].

The measurement would hardly be justified, if the registration of the minumum differences in the currents from the two opposite collectors under changes in the most sensitive scale and the registration of the minimum differences of the same currents in the coarsest scale is not made with the same sensitivity. This is also valid for the maximum differences (from order to order of current) in the entire range of the measured value. Therefore, the device was developed on the basis of logarithmic amplifiers. It contains two identical measurement tracks (Fig. 1) 1 and 2, i. e. one for each couple of opposite collector sections. Therefore, it is sufficient to examine only one of the measuring tracks.

Two cases are possible:

1. The current variations of the four-section separated collector occur within the range of $I=(1.10^{-11} \div 1.10^{-7})$ A. Then I_1 and I_2 enter the inputs of the two current-voltage converters (CCV_1 and CCV_2), at the outputs of which we obtain respectively U_1 and U_2. At the outputs of the next voltage logarith-

mic amplifiers (LA_1 and LA_2) we obtain voltages which enter the two inputs of the differential amplifier DA_1 and thus we obtain at its output:

(1) $$U_g = klg\frac{I_1}{I_2}.$$

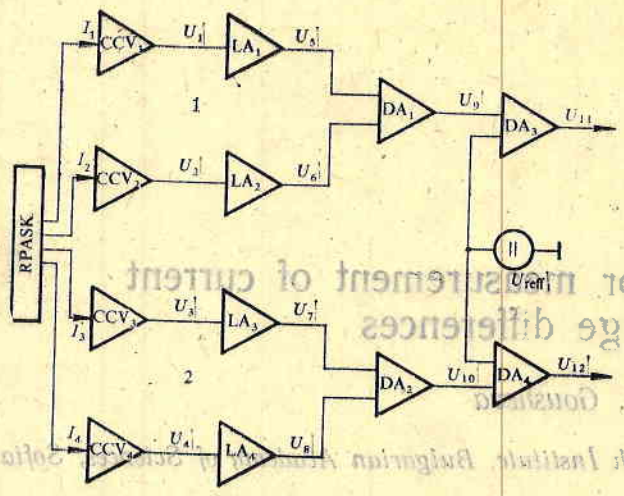

Fig. 1

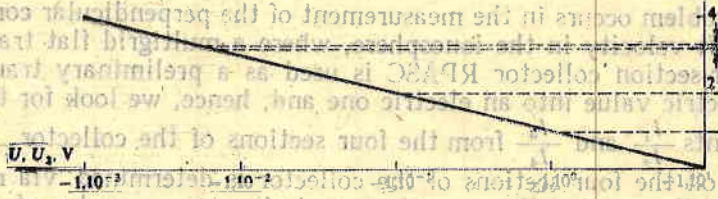

Fig. 2.

We can illustrate two concrete examples for the registration of the current differences (Fig. 2):

a) Ug' for $\Delta I = 1.10^{-11}$ A;

b) Ug'' for $\Delta I =$ (an order).

Besides, the minimum differences inside the scales (for all the scales and from scale to scale) are equal. The minimum differences which can be measured attain 1.10^{-11} A and the maximum — 4 current orders (from $1.10^{-11} \div 1.10^{-7}$) A.

2. The current variations form the four-section collector are within the range of $I = (1.10^{-9} \div 1.10^{-3})$ A. Then, $CCV_{1\div4}$ are not necessary (Fig. 1) and voltage $LA_{1\div4}$ are replaced by current ones. The minimum differences which can be measured then are 1.10^{-9} A and the maximum are 6 orders of the current (from $1.10^{-9} \div 1.10^{-3}$) A.

The measurement of voltage differences is also made with the block-circuit from Fig. 1, without $CCV_{1\div4}$.

The switching on of a reference source of voltage to the inverting input of the differential amplifier DA_3 provides a possibility of shifting the zero of the service telemetric system. Thus, the increase of one of the currents and

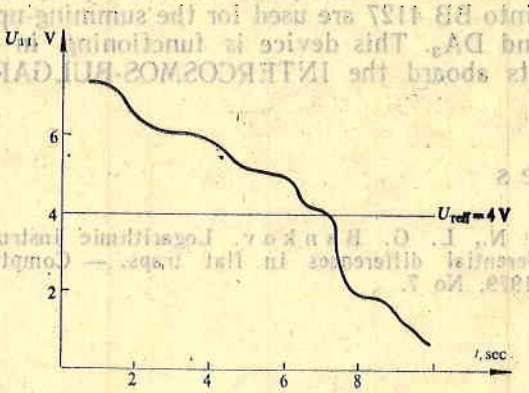

Fig. 3.

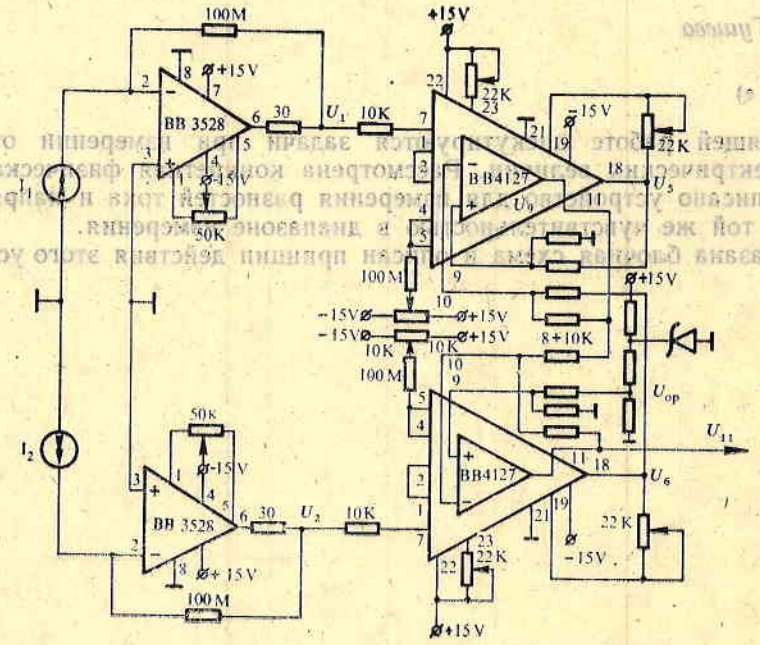

Fig. 4.

the respective decrease of the other (voltage respectively) and the reverse process are easily registrated as

$$U_{11}=k\lg\frac{I_1}{I_2}-U_{tef}. \tag{2}$$

Let $U_{tef}=4$V (Fig. 3). When the currents are equal, $U_{11}=4$V increases up to 8 V and decreases down to 0 V, in dependence on which one of the two currents increases.

A concrete version of the device is shown in Fig. 4. Burr-Brown's preamplifiers BB 3528 are used as CCV. The logarithmic amplifiers in voltage measurement mode BB 4127 are made by the same company. The in-built operational amplifiers into BB 4127 are used for the summing-up of the differential amplifiers DA_1 and DA_3. This device is functioning in the instrument for drift measurements aboard the INTERCOSMOS-BULGARIA-1300 satellite.

References

1. Gusheva, M. N., L. G. Bankov. Logarithmic instrument for measuring small differential differences in flat traps. — Compt. rend. Acad. Bulg. Sci., 32, 1979, No 7.

Устройство для измерения разности тока и напряжения

М. Н. Гушева

(Резюме)

В настоящей работе дискутируются задачи при измерении отношения двух электрических величин. Рассмотрена конкретная физическая ситуация и описано устройство для измерения разностей тока и напряжения с одной и той же чувствительностью в диапазоне измерения.

Показана блочная схема и описан принцип действия этого устройства.

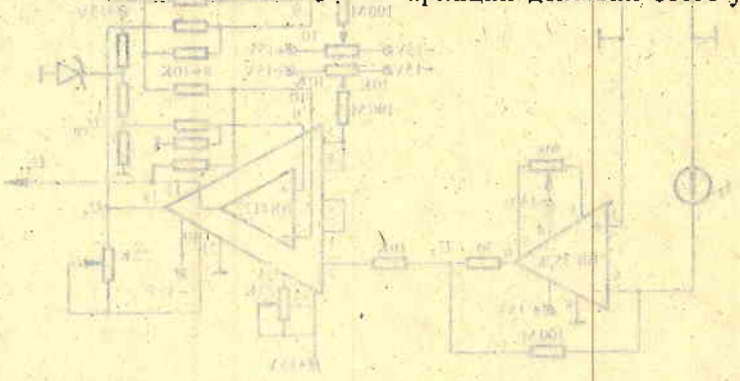

Bulgarian Academy of Sciences

Space Research in Bulgaria, 6

Sofia . 1990

On some specifics in the selection of glass material for microchannel plates in space applications

*Yanko B. Dimitriev, Julika M. Simeonova**

Higher Institute of Chemical Technology, Sofia
**Space Research Institute, Bulgarian Academy of Sciences, Sofia*

The great interest in microchannel plates (MCP), particularly attributed to their space applications, is based on the successful combination of several substantial parameters determining their large functional capacity. However, the latter strongly depend on many factors, such as selection and production of the glass material and its further processing, on the technology of microchannel structure, on the operation mode, and the manner of storing MCP, etc.

The purpose of this paper is to discuss some peculiarities of the glass material which may affect the operational parameters of the MCP, especially during their continuous exposure in space.

Laboratory tests affirm that, regardless of the preliminary treatment of the plates in vacuum medium in order to degas them, they continue to release gases [1]. The curves revealing the kinetics of residual gas release in some spectral lines for plates performing in high vacuum also confirm this [2]. It should be expected that gas release would take place in space too and would affect the operational parameters. This assumption is corroborated by the established effect of gas admixture in glass on the coefficient of amplification of secondary channel multipliers, together with the contribution of glass-dissolved water [3].

Glass is widely applied material in electrovacuum production. Therefore, the attention to gas composition and diffusion in glass might be easily understood. It is known that already in the process of glass synthesis there are residual amounts of H_2O, CO_2, O_2, H_2, $N_2(CO)$, etc. [4]. Besides, the final product absorbs gases on its surface, which may diffuse. During the glass heating up to 300° C in vacuum, the absorbed gases and water are released from its surface and subsurface layers, while those dissolved in the bulk material evolve at higher temperatures [4-6]. The glass structure and the initial content of OH-groups in it affect water diffusion [7, 8]. The glass state — quenched

or tempered — is also of particular importance [5]. Water incorporation and release in glass can be described with the following reaction:

$$H_2O+(\equiv Si—O—Si\equiv)=2(\equiv Si—OH)$$

Predominant is the opinion that at low content of glass-dissolved water (below 0,1%) it is completely manifested by OH-groups [9-11].

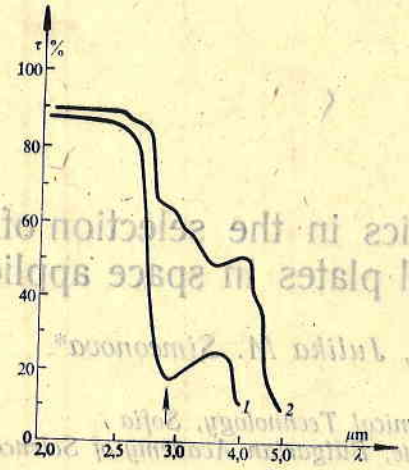

Fig. 1. Dependence of the transmission coefficient on the wave length for two glass compositions

The transmission (absorption) spectra of light in the near infrared region allow to determine the presence of OH-groups and the extent of their relationship with the other structural units in glass. The absorption peak at 2,8 μm (3550 cm^{-1}) could be assigned to the fundamental stretching vibrations of OH [12]. Consequently, these spectra could be used for testing water composition in glass and for selecting glass composition for MCP designed for long exposure in high vacuum, i. e. for space applications.

As an example we shall examine the transmission spectrum of two different lead-silicate glass compositions used in MCP technology. The first material *(1)* contains SiO_2, PbO, B_2O_3, and Bi_2O_3 and Al_2O_3. Its spectrum is shown in Fig. 1 and is specified with an intense absorption peak at 2,7-2,9 μm, typical for OH-groups. The latter do not contribute to the formation of hydrogen bonds. The second material *(2)* contains, besides the mentioned components, Na_2O and K_2O. Its spectrum is much more complex in terms of the examined region. Due to the weaker absorption within the range of 2,7-4 μm, we may assume that the water content is smaller. The complex nature of the spectrum may be assigned to the existence of modifying cations generating non-bridge oxygen bonds within the glass network. This leads to the formation of stable hydrogen bonds between Si-OH and the non-bridge oxygen ions. As a result, the absorption maximum (the maximum in the transmission spectrum) is displaced towards longer wave lengths.

It may be concluded, therefore, that with the introduction of additional modifying oxides in the glass material, it is possible to control the total amount of water and the extent of its bondage in the glass. This is of prime im-

portance for its further behaviour along the MCP exploration. The proper selection of the glass material should ensure the stable amplification of microchannel plates during their continuous performance in space vacuum.

References

1. Boutot, J., — Acta Electr., **14**, 1971, No 2, 245.
2. Кънев, В., К. Пупов, Ю. Симеонова, М. Младенов. — Годишник ВУЗ, сер. тех. физ., т. **18**, кн. 2, 1981, стр. 113.
3. Blasek, G., D. Gütter. — Exper. Techn. Phys., **22**, 1974, 597.
4. Павлушкина, Н. М. Химическая технология стекла и ситаллов. М., 1983.
5. Дешман, С. Научные основы вакуумной техники. М., Мир, 1964.
6. Грошковский, Я. Техника высокого вакуума. М., Мир, 1975.
7. Frichat, G. H. Ionic Diffusion in Oxide Glasses. — Trans. Techn. Public., 1975, p. 34.
8. Brückner, R. — Glastechn., **38**, 1965, 153.
9. Scholze, H. — Glass Ind., **47**, 1966, 622.
10. Bartholomew, R. F., B. L. Butler, H. L. Hoover, C. K. Wu.— J. Amer, Cer. Soc., **63**, 1980, No 9-10, 481.
11. Stopler, E. — Contrib. Mineral Petrol., **81**, 1982, No 1, 1.
12. Scholze, H. — Glastechn. Ber., **32**, 1959, pp. 81, 145 and 278.

О некоторых особенностях при выборе стекла для микроканальных пластин, работающих в космосе

Я. Б. Димитриев, Ю. М. Симеонова

(Резюме)

Некоторыми авторами было установлено влияние растворенной в стекле воды на коэффициент усиления каналовых электронных умножителей. В связи с этим проведено исследование спектра пропускания света через свинцово-силикатное стекло из двух составов в области 2—5 μm, позволяющее получить информацию о присутствии OH-групп и о их связи с остальными элементами структуры. В спектре стекла, содержащего SiO_2, PbO, B_2O_3, Al_2O_3 и Bi_2O_3, обнаружен интенсивный адсорбционный пик (2,7—2,9 μm), который характерен для OH-групп, не образующих водородных связей. Спектр другого стекла, содержащего еще Na_2O и K_2O, сложнее из-за присутствия модифицирующих катионов и его поглощение более слабое. Следовательно внесением дополнительных модифицирующих окислов в стекло можно регулировать общее количество воды и степень ее связанности, что существенно при выборе стекла для микроканальных пластин со стабильным усилением при продолжительной работе в условиях космического вакуума.

Bulgarian Academy of Sciences

Space Research in Bulgaria, 6

Sofia . 1990

Functional generator capacity increase via new building elements

*Nikola B. Tabov, Ivan A. Kurtev**

Institute of Mechanics and Biomechanics, Bulgarian Academy of Sciences, Sofia
**V. I. Lenin Higher Mechanical and Electrical Engineering Institute, Sofia*

Electrostatic particle analyzers range among the widest spread components of space equipment. There exists a great variety both in construction developments: flat, cylindric or semispheric deflectors, quadripole analyzers, linear focussing and amplifying systems, spherical and cylindric probes, and in the problems to be resolved with them. In any case, the operational principle is based on the fact that a voltage is applied betwen the electrodes of an electrostatic system which generates an electric field of selected parameters (direction and voltage) in a specified area. The charged particles trapped into this area are subject to the field effect, their response is an indication for their examined parameter: charge, energy, and mass.

Under different measurements and configuration, the voltage applied between the electrodes of the system is most diverse in form: linearly varying, sawtooth, exponential, step-like, etc.

Some specific requirements for the electronic space equipment should be met by the voltage generators: small size, light weight, low power consumption, high reliability. Sometimes, however, the maximum values of the voltage are significant, of the order of KW, hence, the above mentioned requirements become a serious problem.

A frequently used approach in the design of such generators employs intermediate convergence into voltage of significantly higher frequency, modulated by a driving signal and amplified via transformer to the necessary level, after which the signal in the secondary side of the transformer is detected to reconstruct the shape of the driving signal. The stabilization of the output amplitude is achieved via a comparing amplifier and a negative feedback.

The criticism with regard to this implementation refers mainly to the transformer, due to its relatively large size and weight, and complicated technological production, especially that of the secondary wiring: large number of wires, high-voltage insulation, etc. The optimum efficiency of the used trans-

formers is obtained below 30 KHz which, in turn, is accompanied by higher values of the filter condenser. The energy losses are thus unjustifiably great, especially keeping in mind that the serviced device is electrostatic, i. e. with almost zero consumption.

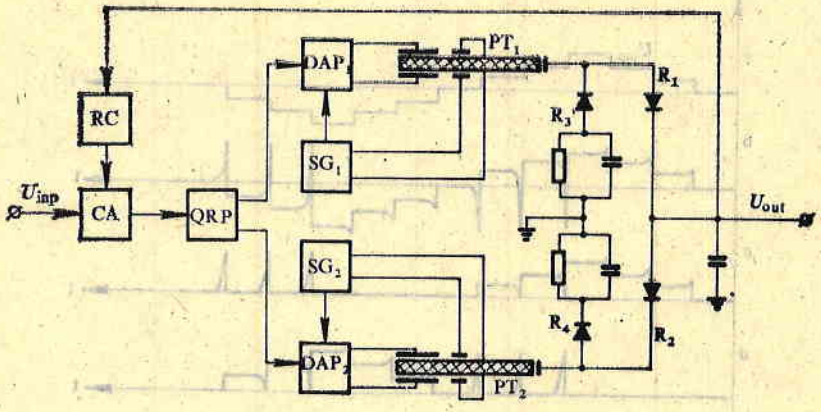

Fig. 1

In the search of new solutions, great prospects are opened by piesoceramics, the material of our century. The use of piesoelectric transformers of voltage with low-charge capacity is quite suitable in electrostatic devices: the components are simple and highly technological, the weight is abruptly reduced, as well as the size and power consumption. The generator described in [1] is of much better qualities than the generators with feromagnetic transformers. The resonance frequencies, being at the same time operational frequencies of the piesotransformers and producing the optimum efficiency together with the maximum coefficient of transmission by voltage, are samples of 30 to 70 mm length and 1 mm thickness within the limits of 30 to 200 kHz.

The converting part of the above two types of generators plays the role of a voltage amplifier. Unfortunately, in both cases the high-voltage amplifiers thus developed do not have all the advantages of the low-voltage electronic amplifiers: they are of single polar output, and the steepness of the descending slopes is significantly worse than that of the ascending ones for the pulse signal reproduction, since it is determined by a time constant of the output circuits throughout the discharge process.

On the basis of piesoelectric voltage transformers a high-voltage amplifire with bipolar output and improved steepness of the descending slopes may be developed [2]. Its block diagram is shown in Fig. 1 and the operation principle is the following: let a bipolar voltage of stepwise form (shown in Fig. 2a) be produced into the low voltage part of the generator (not shown in the Figure). This voltage enters one of the inputs of the comparing amplifier CA, at the other input of which a voltage for negative feedback is supplied from the output of the high-voltage part through the reversive converter RC. In dependence on its polarity, the signal from the CA amplifier output is directed by a dividing circuit to polarity SRP or to the driving input of the first driven amplifier of power DAP_1 (for example, under positive polarity) or to the driving input of the second driven amplifier of power DAP_2 (under negative polarity respectively). This signal modulates the signals from the two osci-

llator circuits SG_1 and SG_2 which, being amplified in power by DAP_1 and DAP_2, enter respectively the exciting sectors of the piesotransformers PT_1 and PT_2. The frequency of the oscillators SG_1 and SG_2 is maintained even at the respective resonance frequencies of the piesotransformers PT_1 and PT_2

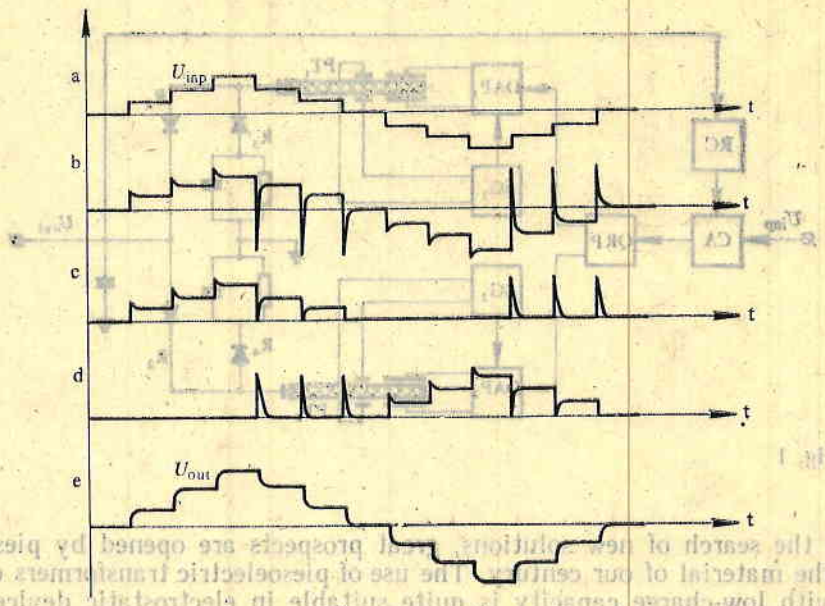

Fig. 2

via the sectors for feedback. For a positive signal with acsending slopes, the driving DAP_1 voltage is zero and PT_2 is not functioning. PT_1 amplifies in resonance mode the signal form DAP_1 which is detected after the output sector of the one-way rectifier for positive polarity R_1. The reconstructed form of the input signal is multiply amplified by voltage, which is defined with the coefficient of transmission of the reversive converter RC.

Thus far, this process does not differ from the performance of known generators. Under descending slopes of the input signal a slow discharge of the output circuits does occur. This delay of the output signal with respect to the input one results in a reverse disbalance at the input of the comparing amplifier CA. The polarity of its output signal changes respectively, namely at the first instant by a value close to that of the supply voltage (Fig. 2c). DAP_1 receives zero at its driving input and PT_1 stops functioning. Then PT_2 starts operating at the output of which a one-way rectifier for negative polarity R_2 is introduced. Thus, active recharge of the output circuits is obtained until the setting of a balance at the input of CA, after which PT_2 is switched off and PT_1 continues its normal performance.

Similar procedures are repeated for the signal of negative polarity at the input, then PT_2 performs normally and the recharging of the output circuits at descending slopes is made via the instantaneous swtching on of PT_1. The piesotransformers PT_1 and PT_2 are not mutually shortened, since their simultaneous operation is not possible and in passive state their output resistance is huge. Supplementary rectifiers R_3 and R_4 are introduced for symmetry. Fig. 2 c, d, e shows the signal shape at the driving inputs of DAP_1 and DAP_2 and at the generator output.

The generator of bipolar output allows to increase the capacity of the equipment and to expand the scope of scientific research, as by one and the same electrostatic device particles of different mass, sign of charge and energy are analysed.

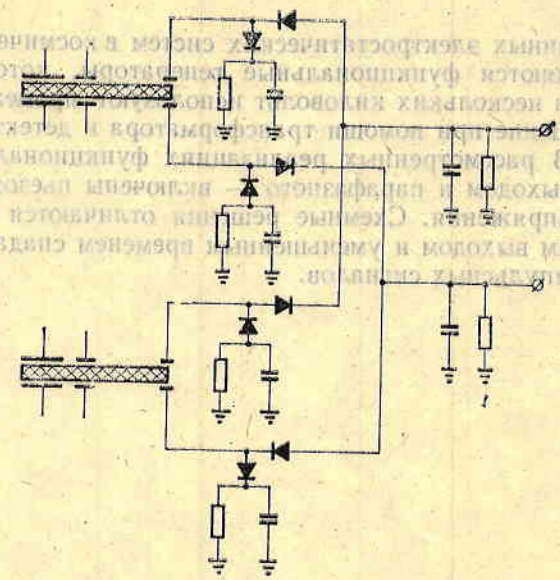

Fig. 3

Using the same block diagram, a paraphase generator [3] may be developed with slight changes. For the purpose, as it is shown in Fig. 3, at each piesotransformer one more output electrode is added, equipotential to the first one, which is simple for technological realization. For the illustrated mode of coupling, two symmetrical paraphase outputs are obtained, as each of them is in addition bipolar and of enhanced fast performance of the descending slopes.

This generator may find applications, for example, in electrostatic deflectors for particle analysis of positive charges as well as of negative. Many applications in other physical instrumentation are possible too.

References

1. Куртев, И., Д. Самоковлийски, С. Стайков, П. Кънев. Източник на високо постоянно напрежение. Авт. свид. на НРБ № 30601 от 30. 05. 80.
2. Табов, Н., И. Куртев, М. Надолийски. Управляем генератор на високо напрежение. Авт. свид. на НРБ № 33254 от 30. 12. 81.
3. Надолийски М., Н. Табов, И. Куртев, Б. Величков. Парафазен генератор на високо напрежение. Авт. свид. на НРБ № 33255 от 30. 12. 81.

Расширение возможностей функциональных генераторов при использовании новых градивных элементов

Н. Б. Табов, И. Ал. Куртев

(Р е з ю м е)

Для питания различных электростатических систем в космической научной аппаратуре применяются функциональные генераторы, которые при напряжениях порядка нескольких киловолт используют промежуточное преобразование, повышение при помощи трансформатора и детектирование выходного сигнала. В рассмотренных реализациях функциональных генераторов — с одним выходом и парафазного — включены пьезоэлектрические трансформаторы напряжения. Схемные решения отличаются от известных своим двухполярным выходом и уменьшенным временем спада фронтов при воспроизведении импульсных сигналов.

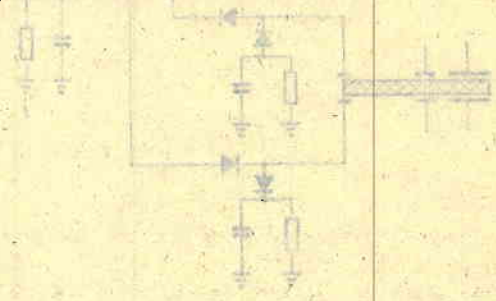

Bulgarian Academy of Sciences

Space Research in Bulgaria, 6

Sofia . 1990

Increase of the efficiency of self-oscillating push-pull power converter

Angel G. Genchev

Space Research Institute, Bulgarian Academy of Sciences, Sofia

Space applications of small-current supply often require improvement of the routine electric circuitry in order to ensure higher reliability. This paper examines the improvement of the energy parameters of the classical converter cell.

The theory and practice of small-current sources broadly imply self-oscillating converters with saturated converting transformers [1]. They are used as driving generators or power transformers of low energy. The block diagram is shown in Fig. 1.

The operating frequency is determined with the following expression:

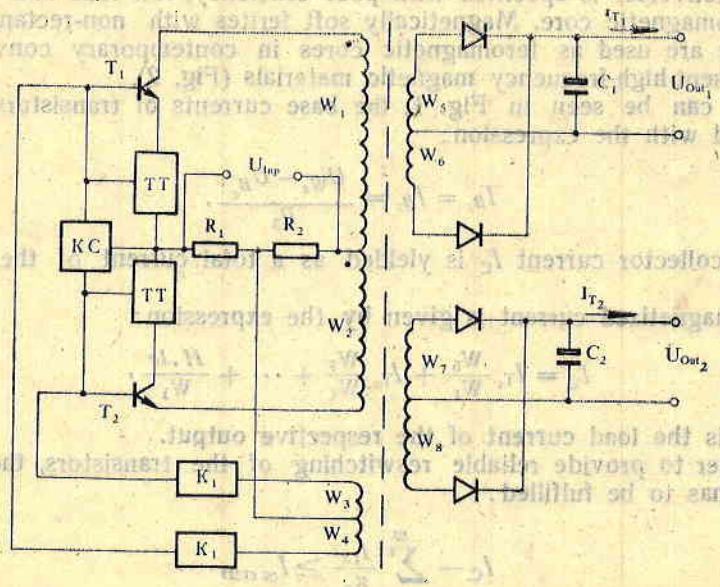

Fig. 1. Standard push-pull self-oscillating converter

(1) $$\frac{dB}{dt} = \frac{(E - U_{CE\,SAt}) \cdot 10^4}{W_1 \cdot Ac},$$

or where

$$f = \frac{1}{T} = \frac{(E - U_{CE\,SAt}) \cdot 10^4}{4\,B_{max} \cdot W_1 \cdot A_E}.$$

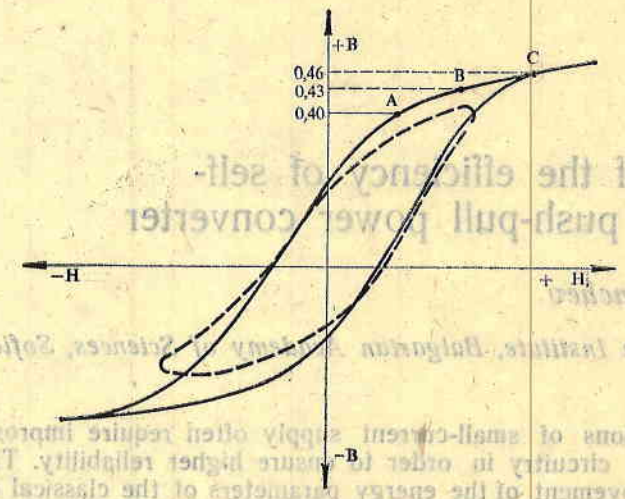

Fig. 2. Histeretic curve for soft magnetic ferrites: at low frequencies (solid line); at high frequencies (dashed line)

This converter is specified with poor efficiency, low load and great losses in the feromagnetic core. Magnetically soft ferites with non-rectangular histeretic curve are used as feromagnetic cores in contemporary converters, i. e. they represent high-frequency magnetic materials (Fig. 2).

As it can be seen in Fig. 1, the base currents of transistors T_1 and T_2 are defined with the expression:

$$I_{B_1} = I_{B_2} = \frac{U_{W_3} - U_{B_e}}{R_3},$$

while the collector current I_C is yielded as a total current of the secondary wiring.

The magnetized current is given by the expression:

(2) $$I_C = I_{T_1} \frac{W_5}{W_1} + I_{T_2} \frac{W_7}{W_1} + \cdots + \frac{H \cdot le}{W_1},$$

where I_{tx} is the load current of the respective output.

In order to provide reliable reswitching of the transistors, the following condition has to be fulfilled:

(3) $$I_C - \sum_{x=1}^{m} \frac{I_{tx}}{\pi_x} \geq I_{m\,crit},$$

where I_{mcrit} is the minimum magnetized current of intensity H at the point of change in the histeretic curve slope. Since $I_{m\,crit}$ is high for such type of converters and a strain of $H \geq 80$ A/m has to be achieved for the most frequently used types [2], then the maximum collector current at weak loading

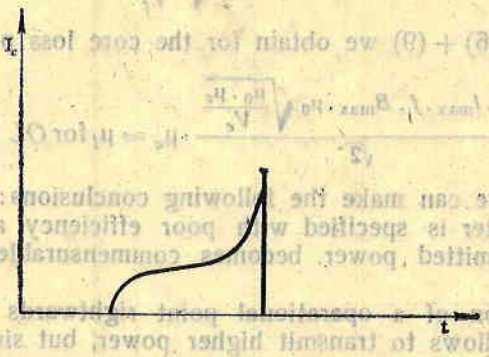

Fig. 3. Collector current shape for saturated transformer converter

of the converter is determined exclusively by the second term of equation (2). The shape of the collector current is shown in Fig. 3.

The maximum value of the collector current is defined with the base current and the amplification index $h_{21\,e}$ for bipolar transistors, and by the gate-source voltage and the preliminary characteristics for the power FET transistor. In addition, in order to obtain great power, the switching-off position is selected rightwards from the histeretic curve (point B and point C), in Fig. 2 which results in a greater increase of losses in the magnetic core, field keys, etc.

The losses in the ferrite core are given with

$$P_c = P_{hist} + P_{sec} + P_{suppl}, \tag{4}$$

where $P_{hist} = \frac{f \cdot \Phi H \cdot dB}{\gamma}$ [W/kg] are the histeretic losses; γ is the density of the material; $P_{sec} \approx 0$ are the losses of the eddy currents. This component for frequencies up to the critical one is negligibly small in ferrites.

P_{suppl} are the supplementary losses effective only for weak fields $H \leq 10$ A/m.

Usually the "angle of losses" parameter is used for the quantitative determination of the losses

$$\operatorname{tg}\delta = \frac{R_s}{\omega L_s} = \delta_{hist} \cdot h + \delta_{sec} \cdot f + \delta_{suppl}, \tag{5}$$

which in agreement with (3) is:

$$\operatorname{tg}\delta = \eta_B \cdot \mu_e \cdot B_{max}/h, \tag{6}$$

where h — histeretic coefficient of the material; η_B — material histeresis constant

The total loss of power in the core may be expressed with

$$P_c = I^2 \cdot l_{max} \cdot R_S = I^2 \cdot l_{max} \cdot \omega L \cdot \operatorname{tg}\delta. \tag{7}$$

We substitute $\operatorname{tg}\delta$ into (7) with its value from (6) and obtain

$$P_c = \frac{I^2 \cdot l_{max} \cdot f \cdot \mu_e \cdot B_{max}}{\sqrt{2} \cdot \mu^2} \text{ [W/kg]}. \tag{8}$$

The core histeresis constant is used to introduce its parameters as related to its geometric size

$$\eta_1 = \mu_e \cdot \mu_B \sqrt{\frac{\mu_0 \cdot \mu_e}{V_e}}. \tag{9}$$

From expressions (6) + (9) we obtain for the core loss power

$$P_c = \frac{I^2 \cdot l_{max} \cdot f \cdot B_{max} \cdot \mu_0 \sqrt{\frac{\mu_0 \cdot \mu_e}{V_e}}}{\sqrt{2}}, \mu_e \approx \mu_i \text{ for } OL \text{ type core.} \tag{10}$$

In summary we can make the following conclusions:

— The converter is specified with poor efficiency at low loading since the usefully transmitted power becomes commensurable with the circuitry losses;

— The selection of a operational point rightwards the point A of the histeretic curve allows to transmit higher power, but simultaneously abruptly increases the losses of the transformer core;

— The field keys are used in a capacity less than complete by current and are subject to overload at the point of switch-off.

The efficiency/output power characteristics may be improved and linearized significantiy with proportional current control of the field keys in dependence on the output power of the converter. A method of increasing the real efficiency of such converters is suggested in [5]. Their general block diagram is given in Fig. 4.

The proportional control is made in agreement with the expression

$$I_b = k \cdot I_k + K_1, \tag{11}$$

where $k = \frac{S}{h_{21e\ min}}$ and $K_1 = \frac{I_m}{h_{21e\ min}} = \frac{H_{crit} \cdot l_e}{W_1 \cdot h_{21e\ min}}$.

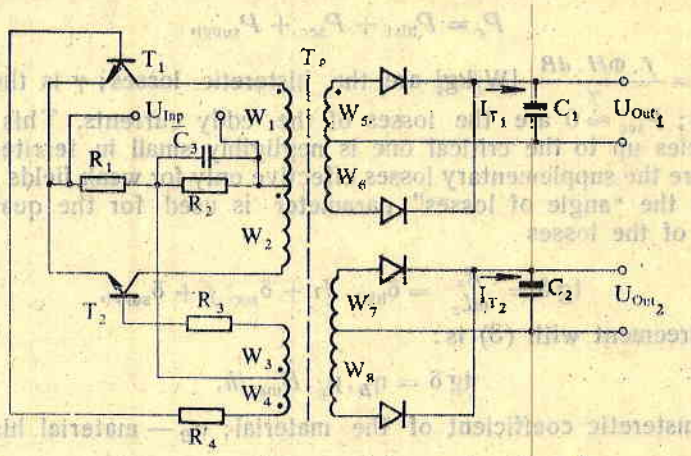

Fig. 4. Generalized block diagram of improved push-pull self-oscillating converter

The proportional feeding of the base is provided with k coefficient, while K_1 determines the minimum strain of field H, in order to safeguard the regenerative operational cycle.

When using advanced MOS transistors, the circuitry is transformed by replacing current transformers with current-to-voltage converters. Expression (11) takes the form of

$$E_{GS} = T_k/g_m + E_{GS\ init}, \quad (12)$$

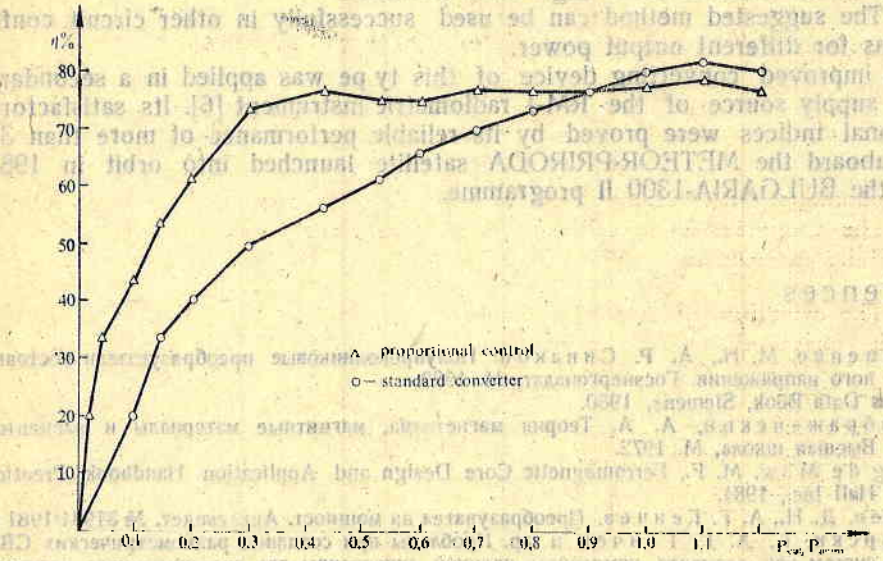

Fig. 5. Experimentally obtained curve, reflecting the efficiency of both converter types in dependence on the normalized output power

where g_m — transistor transadmittance, $E_{GS\ init}$ — prevoltage applied to the gate in order to ensure the required drain current, corresponding to field H_{min}.

We have to apply a thermal compensation of the gate voltage E_{GS} too, since it has a negative temperature coefficient (usually 20-25 mV/C°).

Additionally, for both modifications we have to ensure signal integration proportional to the collector (drain) current at the end of its switched-on position, so as to avoid introduction of a supplementary coefficient in equations (11) and (12) and an avalanche-like current amplification via the transistor.

The advantage of the method described was experimentally verified with the use of a small 15 W inverter. For power transistors, the bipolar 2N5038 and MOS FET VN64GA types were used. In order to provide a correct set-up and to take four reliable measurements, one and the same converting transformer was used: the ferrite core type 30 X 19, T 26, Al 6200, V_e 6100 mm^3

The results from these measurements are shown in Fig. 5 for a bipolar power transistor.

On the basis of theoretical and experimental evidence, we can make the following more important conclusions:

1. The method suggested for the loss decrease in converter with saturated transformer allows to improve by simple means the efficiency coefficient at an average 20 %, when operating with normalized power $P_{out}/P_{norm} < 0{,}5$.

2. At low output power, a converter implemented on powerful MOS transistors has an efficiency $2 \div 4$% higher than the similar converter on bipo-

lar transistors. This is due to the drop of the base power, necessary for the control of the bipolar transistors.

3. Vice versa, at high power the efficiency of the powerful MOS transistors modification is lower, due to the effect of the higher voltage of saturation in these instruments at high drain currents.

4. The suggested method can be used successfully in other circuit configurations for different output power.

An improved converting device of this ty pe was applied in a secondary current supply source of the RM-1 radiometric instrument [6]. Its satisfactory operational indices were proved by its reliable performance of more than 36 month aboard the METEOR-PRIRODA satellite launched into orbit in 1981 within the BULGARIA-1300 II programme.

References

1. Кузьменко, М. Н., А. Р. Сиваков. Полупроводниковые преобразуватели постоянного напряжения. Госэнергоиздат, М. 1980.
2. Ferrites Data Book, Siemens, 1980.
3. Преображенский, А. А. Теория магнетизма, магнитные материалы и элементы. Высшая школа, М. 1972.
4. OOug de Maw, M. F., Ferromagnetic Core Design and Application Handbook, Prentice Hall Inc., 1981.
5. Мишев, Д. Н., А. Г. Генчев. Преобразувател на мощност. Авт. свидет. № 31934/1981 г.
6. Назърски, Т., А. Г. Генчев и др. Проблемы при создании радиометрических СВЧ систем как элемента комплексов научной аппаратуры для дистанционного исследования Земли из Космоса. — Материалы 3-го международного семинара "Научное космическое приборостроение". Москва, 1983.

Повышение коэффициента полезного действия самоосциллирующего двухтактного преобразователя мощности

А. Г. Генчев

(Резюме)

В работе рассматриваются метод и устройство для повышения коэффициента полезного действия стандартного самовозбуждающегося двухтактного преобразователя мощности с насыщаемым трансформатором. Обсуждаются причины, вызывающие ухудшение эффективности преобразователя при низкой нагрузке. Применено техническое решение, позволяющее повысить его эффективность при низкой нагрузке, и представлены экспериментальные результаты.

Bulgarian Academy of Sciences

Space Research in Bulgaria, 6

Sofia . 1990

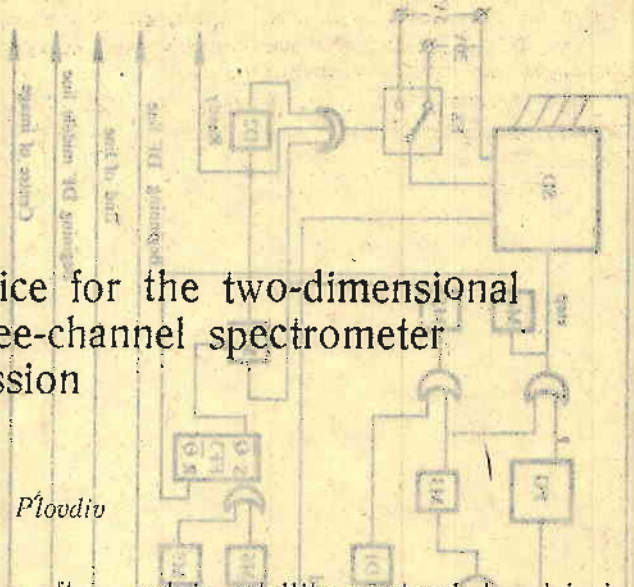

A controllable device for the two-dimensional scanner in the three-channel spectrometer for the VEGA mission

Stoyan I. Sargoichev

Centre of Applied Physics, Plovdiv

Scanning optical systems are often used in satellite spectrophotometric instruments for the study of natural optical emissions. Such a system of Kassegren's type with two-dimensional scanning of the secondary mirror is described in [1]. The angular scanning motion of the secondary mirror is achieved for this system with the aid of an exact small-size scanner, installed behind the mirror [2]. When scanning, the mirror can occupy 105 fixed positions. This corresponds to a sweep containing 7 lines of 15 elements (positions) per line.

The controlling device of the scanning system should interact with a microprocessor system of the instrument and should independently resolve the following problems: 1) performance of the scanner in the linearly-progressive sweep mode — mode A; 2) scanner operation in the linearly-reversive scanning of the middle line — mode B; 3) rapid setting into the initial reference position by a given command; 4) receiving of a command on the modes and signal shaping of completed step; 5) processing — transmission of the sensor system signals for four reference positions of the sweep: beginning of line, end of line, beginning of middle line, sweep centre.

The functional block scheme of the controlling device developed for the purpose is shown in Fig. 1. The following denominations are used: SM — step motor, ST1-ST3 — sensor signals for positioning; STML — sensor signal for middle sweep line; DM1, DM2 — modulating discs, ST — Smith trigger block; M1 ÷ M8 — monovibrators; FF1 — fast/slow rotation trigger of the step driver; FF2 — foreward/backward trigger, PG — pulse generator of the fixed initial phase, SD — servocontrol; ES — electric switch; D1 — retarding "1", D2 — retarding "2".

The circuitry is incorporated as a peripheral device into the microprocessor system of the optical spectrometer. From this system "com step" and "mode A/B" signals are received, and respectively "ready" and the four reference signals of positioning with respect to the sweep are transmitted. When

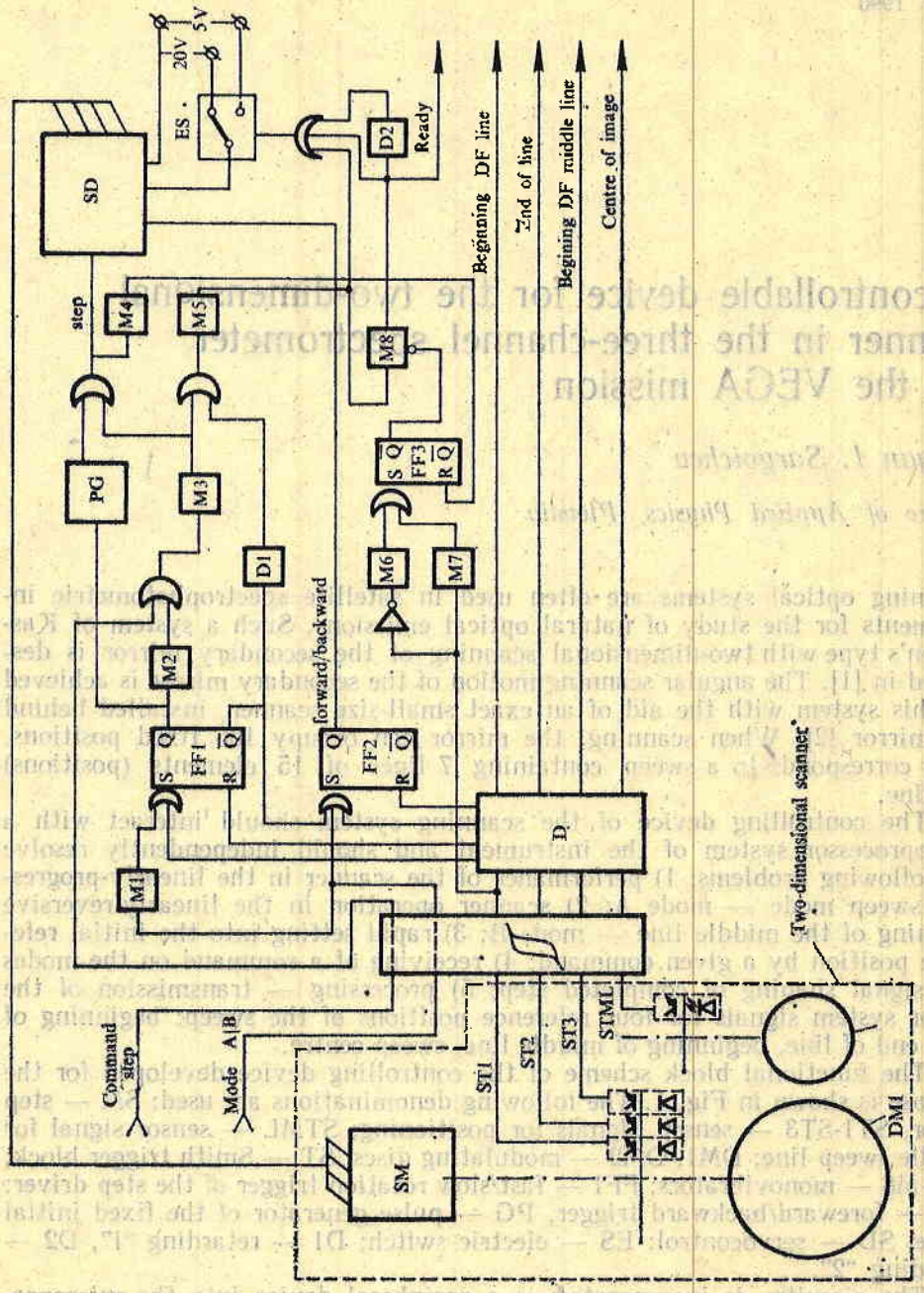
20V
5V
ES
SD
D2
Ready
Beginning DF line
End of line
Begining DF riddle line
Centre of image
step
M4
M5
M8
PG
M3
FF3
D1
forward/backward
M6
M7
M2
FF1
FF2
D
M1
Two-dimensional scanner
Command step
Mode A|B
ST1
ST2
ST3
STML
SM
DM1

Fig. 1

defining the B mode, the controlling device positions automatically the scanner at the beginning of the middle sweep line by fast rotation of the step motor. In A mode, the fast-drive rotation is achieved automatically during the reverse sweep course. The fast-drive rotation pulses are generated by the PG block.

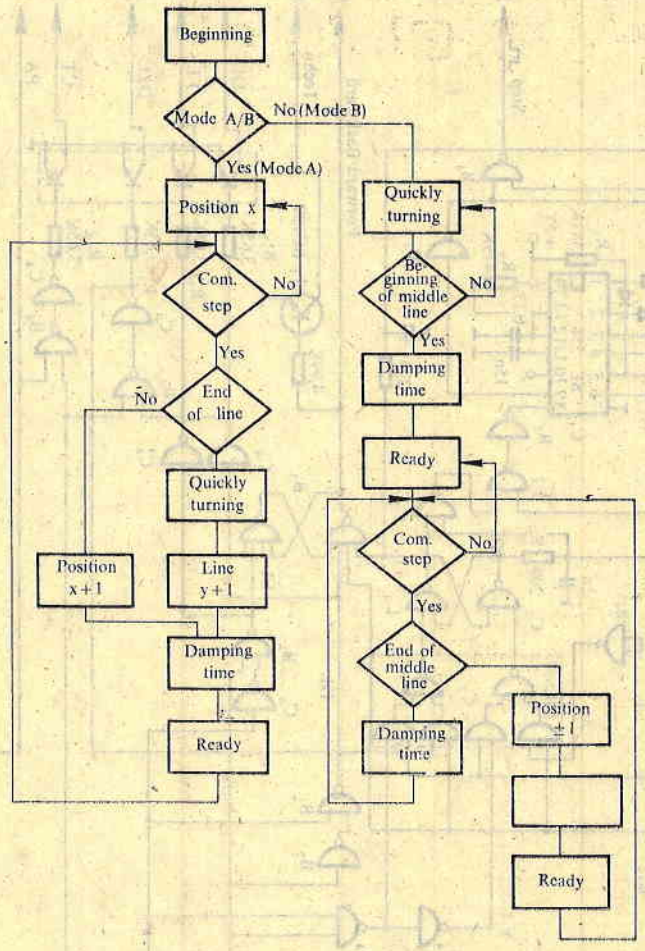

Fig. 2

With the aid of the non-contact key ES the supply voltage is reswitched, and hence the total current via the driver during rotation and in a fixed position, thus reducing the average power consumption. The output signals for the scanner position with regard to the sweep are shaped by its sensor system signal decoding. The DM1 modulator disc contains three tracks, optically connected with three optocouples — light-diode phototransistor with diaphragms. The DM2 disc contains an aperture for angular reference. When the information from the outer and middle DM1 tracks is decoded, we obtain the output signals "beginning of line" and "end of line", as well as the inner signals for the direct and reverse sweep course via the ST1 and ST2 sensors. The signals are

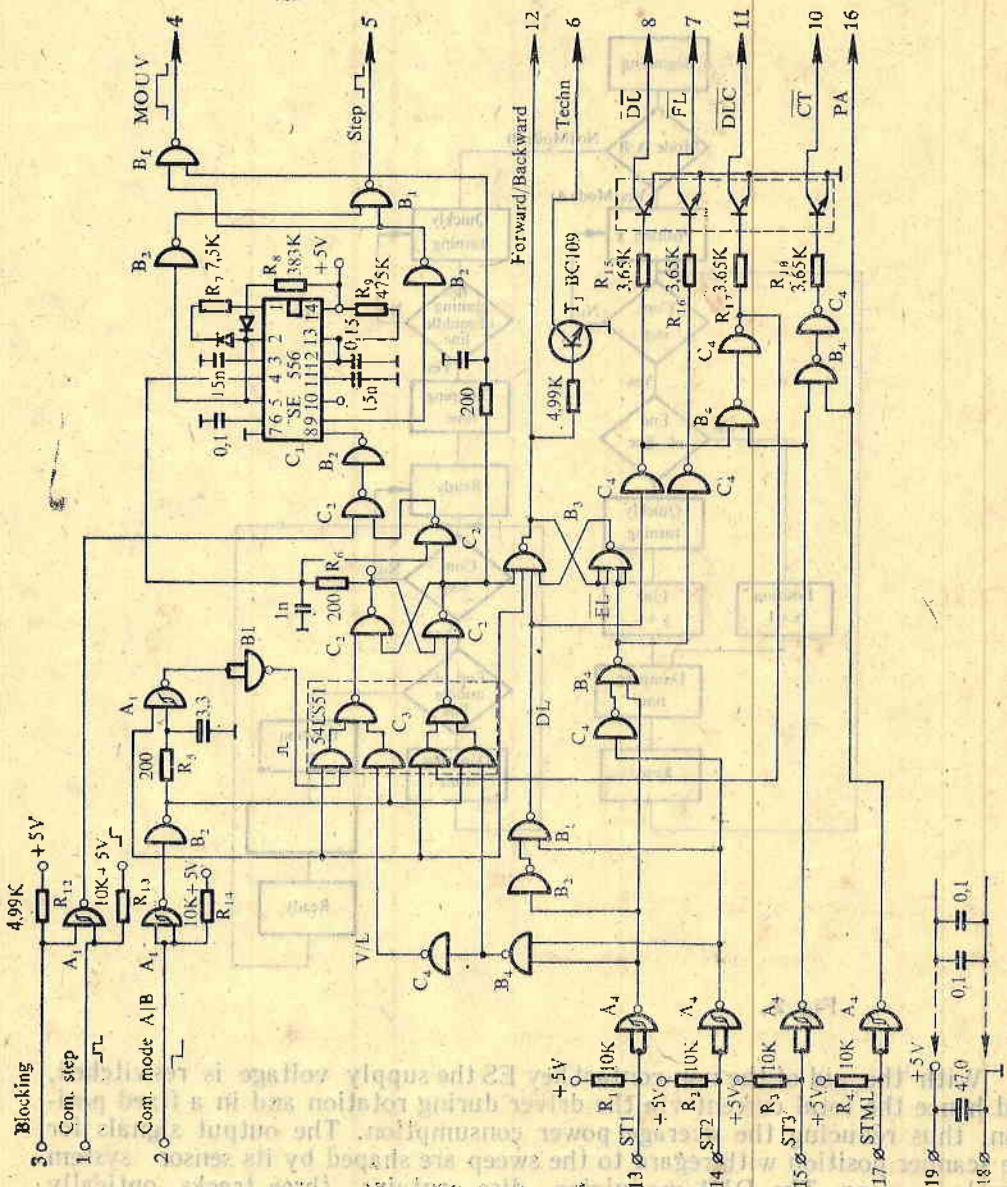
MOUV
Step
Forward/Backward
Techn
DE
FL
DLC
CT
PA
DL
EL
V/L
B1
T1 BC109
4,99K
Blocking
Com. step
Com. mode A/B
ST1
ST2
ST3
STM1
+5V

Fig. 3

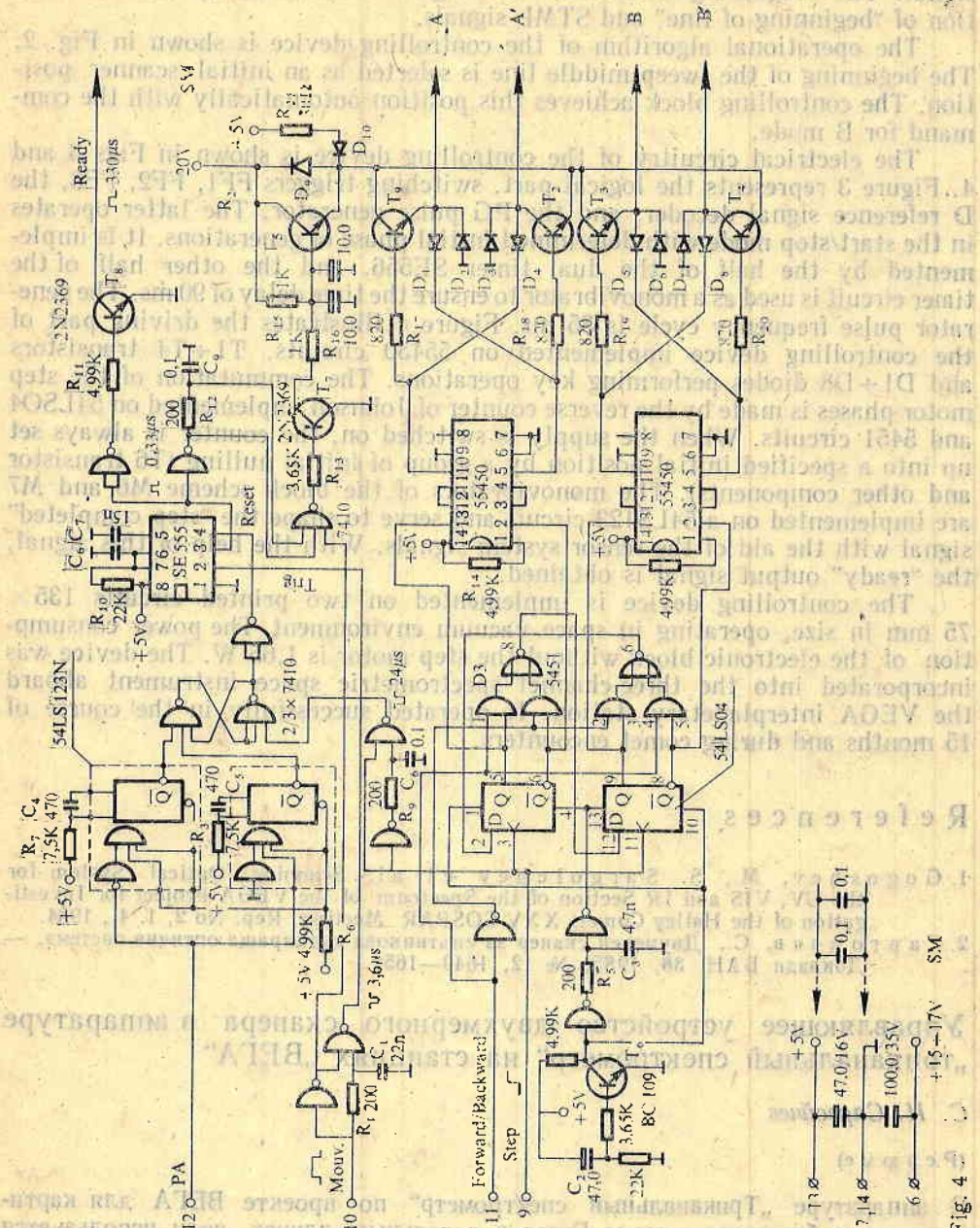
A
A'
B
B'
Ready
330µs
2N2369
SE 555
Reset
0,33µs
3,65K
7410
2,3× 7410
24µs
3,6µs
54LS123N
54LS04
7,5K
4,99K
22K
200
820
10,0
0,1
22n
4,7n
47,0
3,65K
BC 109
5451
55450
PA
Mouv.
Forward/Backward
Step
SM
+5V
+15–17V
47,0/16V
100,0/35V

Fig. 4

transmitted to the M1, FF1 and FF2 blocks. The "ready" signal is obtained from the inner track through appropriate electron processing in blocks M6, M7, FF3 and M8. In addition, the combination with STML signal provides the „centre of image" signal. The "beginning of middle line" signal is obtained by the combination of "beginning of line" and STML signals.

The operational algorithm of the controlling device is shown in Fig. 2. The beginning of the sweep middle line is selected as an initial scanner position. The controlling block achieves this position automatically with the command for B mode.

The electrical circuitry of the controlling device is shown in Figs 3 and 4. Figure 3 represents the logical part, switching triggers FF1, FF2, FF3, the D reference signal decoder, and the PG pulse generator. The latter operates in the start/stop mode with determined initial phase of generations. It is implemented by the half of the dual timer SE556, and the other half of the timer circuit is used as a monovibrator to ensure the time delay of 90 ms. The generator pulse frequency cycle is 35 ms. Figure 4 illustrates the driving part of the controlling device implemented on 55450 circuits, T1÷T4 transistors and D1÷D8 diodes performing key operations. The commutation of the step motor phases is made by the reverse counter of Johnson implemented on 54LSO4 and 5451 circuits. When the supply is switched on, the counter is always set up into a specified initial position by a group of initial nulling (T6 transistor and other components). The monovibrators of the block scheme M6 and M7 are implemented on a 54LS123 circuit and serve to shape the "step completed" signal with the aid of the sensor system signals. With the help of this signal, the "ready" output signal is obtained.

The controlling device is implemented on two printed circuits 135×75 mm in size, operating in space vacuum environment. The power consumption of the electronic block without the step motor is 1,65 W. The device was incorporated into the three-channel spectrometric space instrument aboard the VEGA interplanetary station. It operated successfully in the course of 15 months and during comet encounters.

References

1. Gogoshev, M., S. Sargoichev et al. Scanning Optical System for the UV, VIS and IR Section of the Spectrum of the VEGA Project for Investigation of the Halley Comet. XXV COSPAR Meeting, Rep. No 2. 1. 4., 1984.
2. Саргойчев, С., Двумерен сканер за спътникова сканираща оптична система. — Доклади БАН, 38, 1985, № 12, 1649—1652.

Управляющее устройство двухмерного сканера в аппаратуре „триканальный спектрометр" на станциях „ВЕГА"

С. И. Саргойчев

(Резюме)

В аппаратуре „Триканальный спектрометр" по проекте ВЕГА для картирования изображения кометы Галея в отдельных длинах волн используется телескопическая система с механическим двухмерным сканированием изображения. Объектом рассмотрения в настоящей работе является управляющее устройство для механического сканера. Представлены функциональная блок-схема, алгоритм управления и принципиальные схемы этого устройства.